https://doi.org/10.61092/iaea.r0ba-4gsw

INDC(NDS)-0904
Distr. RD,ST,PH

IAEA
International Atomic Energy Agency

INDC International Nuclear Data Committee

Impact of Photonuclear Reactions on Neutron Dosimetry in ^{252}Cf(s.f.) and ^{235}U(n_{th},f) Neutron-gamma Mixed Radiation Fields

S. Simakov

Karlsruhe Institute of Technology
Eggenstein-Leopoldshafen, Germany

October 2024

IAEA Nuclear Data Section
Vienna International Centre, P.O. Box 100, 1400 Vienna, Austria

Selected INDC documents may be downloaded in electronic form from
http://www-nds.iaea.org/publications
or sent as an e-mail attachment.
Requests for hardcopy or e-mail transmittal should be directed to
NDS.Contact-Point@iaea.org
or to:
Nuclear Data Section
International Atomic Energy Agency
Vienna International Centre
PO Box 100
1400 Vienna
Austria

INDC(NDS)-0904
Distr. RD,ST,PH

Impact of Photonuclear Reactions on Neutron Dosimetry in ^{252}Cf(s.f.) and ^{235}U(n_{th},f) Neutron-gamma Mixed Radiation Fields

S. Simakov

Karlsruhe Institute of Technology
Eggenstein-Leopoldshafen, Germany

Abstract

The systematic analysis of the competition between the γ-ray induced and the neutron dosimetry reactions in the ^{252}Cf(s.f.) and ^{235}U(n_{th},f) mixed neutron-gamma radiation fields was performed for the first time. 49 neutron induced reactions on mono-isotopes in the IRDFF-II library were found for which the photonuclear reactions produce the same residual or observable. The following competing reaction pairs were eventually considered: (n,f) and (γ,f), (n,n') and (γ,γ'), (n,xn) and (γ,(x-1)n) with neutron multiplicity x = 2 – 10, (n,np+d) and (γ,p), (n,α) and (γ,h). The contributions were quantitatively estimated using the calculated gamma and neutron Spectrum Averaged Cross Sections (SACS). The energy spectra and multiplicities for the ^{252}Cf(s.f.) and ^{235}U(n_{th},f) radiations where taken either from nuclear standards (e.g., prompt fission neutron spectra) or from available evaluations (e.g., fission gamma spectra) which are presently known up to 20 – 30 MeV. Both the prompt and delayed radiation emission modes were considered. Extrapolation of the radiation energy distributions for ^{252}Cf(s.f.) and ^{235}U(n_{th},f) up to 100 – 200 MeV was made based on the energy trends or scarce existing experimental data. Eventually the impact of (γ,x) on the total residual production was shown to be less than ≈ 1% for most of the considered reaction pairs and thus could be neglected since 1% is the highest accuracy presently achievable. The role of the photonuclear reaction increases and becomes dominating for the high threshold reactions such as (γ,(x-1)n) and (n,xn) on ^{209}Bi when x ≥ 5, if the energy distribution of gammas from ^{252}Cf(s.f.) and ^{235}U(n_{th},f) tends to plateau at energies above ≥ 40 MeV.
In addition to the mono-isotope targets, the natural elements which are also included in IRDFF-II were considered. 13 elements were found, where, additionally to the neutron dosimetry reactions on specific isotopes, the photonuclear reactions on other isotopes will contribute to the radionuclide production. Such an impact was estimated to be lower than 10^{-4}% and can be safely neglected in neutron dosimetry.

October 2024

Contents

1. Introduction

The International Reactor Dosimetry and Fusion File (IRDFF-II) [1] is an internationally recognised library of reference neutron induced cross sections. It is widely used by the dosimetry community in various research and power reactor applications. IRDFF-II relies on the microscopic cross section measured data and IRDFF-II evaluations were validated in the standard or reference neutrons fields such as the Prompt Fission Neutron Spectra (PFNS) from reactions ^{252}Cf(s.f.), ^{235}U(n_{th},f) and other more complicated fields [1]. This validation was performed by comparison of the measured and calculated neutron induced Spectrum Averaged Cross Sections (SACS). The abbreviation SACS was so far traditionally used for neutron reactions and fields. In the present work we will designate it as n-SACS to distinguish from the γ-spectra averaged gamma induced cross sections γ-SACS.

The ^{252}Cf(s.f.) and ^{235}U(n_{th},f) radiation sources emit additionally to neutrons also gammas. The gamma multiplicities per fission event are even several times larger than the neutron ones. If the neutron and gamma induced reactions on a given target isotope result in the same final reaction product (residual radionuclide or fission fragments, used for the reaction detection), then the neutron and gamma induced contribution become impossible to separate experimentally. Such an impact of gammas has not yet been investigated for the refence neutron fields, in particular because the accompanying gamma spectra were not well studied and numerically characterized or because the role of gammas was ignored.

The purpose of the present work is a systematic study of the competition between the neutron and gamma induced reactions leading to the same residuals in the ^{252}Cf(s.f.) and ^{235}U(n_{th},f) gamma-neutron mixed fields. For all neutron reactions included in IRDFF-II, the competing gamma reaction were searched. The following pairs were found, for which the impact wasα estimated: (n,f) and (γ,f), (n,n') and (γ,γ'), (n,xn) and (γ,(x-1)n) where x = 2 - 10, (n,pn+d) and (γ,p), (n,α) and (γ,^{3}He). Since activation measurements span the time typically more than seconds, both the prompt and delayed emission modes, i.e. their multiplicities and energy spectra, were considered for neutrons and gammas.

In practice, the dosimetry samples consisting of the single natural (but non mono-isotope) element are often used. However, the neutron induced reaction only on single isotope of element is considered as neutron dosimeter in IRDFF-II. In these cases, the photonuclear reactions on all other isotopes of element could result in production of the same reaction residual as the IRDFF neutron dosimeter. Such influence of the photonuclear reactions in the elemental targets was found only for the neutron dosimetry reactions (n,2n), (n,p) and (n,α), their contribution was estimated too.

This is the first systematic study of the impact of the photonuclear reaction on the residual production by the neutron dosimetry reaction in the reference ^{252}Cf(s.f.) and ^{235}U(n_{th},f) radiation mixed fields. First our attempts were undertaken in [2], where the competition between the (γ,n) and (n,2n) production pathways on the ^{238}U and ^{24}Na targets in the ^{235}U(n_{th},f) mixed radiation field was calculated.

Section 2 of this report describes the cross section libraries, reaction identifications and processing used in the calculations; Section 3 gives an overview of the status of the existing neutron and gamma energy spectra and averaged multiplicities for the ^{252}Cf(s.f.) and ^{235}U(n_{th},f) mixed radiation fields and extension to the higher emission energies; Section 4 reports the calculated neutron- and gamma-induced spectrum average cross sections, yields and partial fractions to the total residual production; Section 5 shows the impact of (γ,x) reactions in the case of elemental targets; Section 6 shortly investigates the feasibility to measure the extremely high energy threshold reactions on ^{209}Bi. The report concludes with a summary.

2. Cross sections for the competing neutron and gamma induced reactions

This section gives an overview of the neutron and gamma induced cross section libraries, the identification of reaction type and necessary data processing used for the calculation of the spectrum averaged cross section and, eventually, for the estimation of the impact of photonuclear reactions on neutron dosimetry.

Table 2.1 lists 43 neutron dosimetry reactions found in the IRDFF-II library [1], explicitly those for which the competing photonuclear reactions found in the IAEA/PD-2019.2 [3] or TENDL-2023 [4] libraries result in the same residual. Most of these pairs lead to the final unstable nuclei decaying with emission of bettas or gammas, the latter are used to measure the reaction cross section. To this list of competing reactions the fission reactions

(n,f) and (γ,f) are also added, since detectors of the fission fragments (FF) cannot distinguish between incident neutrons and photons.

TABLE 2.1. Neutron induced dosimetry reactions on mono-isotopes from the IRDFF-II library and competing gamma induced reactions from IAEA/PD-2019.2 or TENDL-2023.
(Column "Thresh" contains the reaction kinematic thresholds, "MF/MT/ZAP" - the MF, MT and product ZAP numbers which were used to invoke the required cross sections from the used evaluated cross section library.)

Neutron induced reaction				**Gamma induced reaction**			
Reaction	Thresh, MeV	Library	MT or ZAP	Reaction	Thresh, MeV	Library	MF/MT /ZAP
(n,f) and (γ,f) reactions leading to the fission and similar Fission Fragments (FF)							
^{230}Th(n,f)FF	0.0	IRDFF-II	18	^{230}Th(γ,f)FF	0.0	IAEA/PD-2019	18
^{235}U(n,f)FF	0.0	IRDFF-II	18	^{235}U(γ,f)FF	0.0	IAEA/PD-2019	18
^{238}U(n,f)FF	0.0	IRDFF-II	18	^{238}U(γ,f)FF	0.0	IAEA/PD-2019	18
^{237}Np(n,f)FF	0.0	IRDFF-II	18	^{237}Np(γ,f)FF	0.0	IAEA/PD-2019	18
^{239}Pu(n,f)FF	0.0	IRDFF-II	18	^{239}Pu(γ,f)FF	0.0	IAEA/PD-2019	18
^{241}Am(n,f)FF	0.0	IRDFF-II	18	^{241}Am(γ,f)FF	0.0	TENDL-2023	18
(n,n') and (γ,γ') reactions on the same target and leading to production of the same isotope							
^{93}Nb(n,n')^{93m}Nb	0.031	IRDFF-II	41093m	^{93}Nb(γ,γ')^{93m}Nb	0.031	IAEA/PD-2019	41093m
^{103}Rh(n,n')^{103m}Rh	0.040	IRDFF-II	45103m	^{103}Rh(γ,γ')^{103m}Rh	0.040	TENDL-2023	45103m
^{113}In(n,n')^{113m}In	0.395	IRDFF-II	49113m	^{113}In(γ,γ')^{113m}In	0.392	TENDL-2023	49113m
^{115}In(n,n')^{115m}In	0.339	IRDFF-II	49115m	^{115}In(γ,γ')^{115m}In	0.336	IAEA/PD-2019	49115m
^{199}Hg(n,n')^{199m}Hg	0.535	IRDFF-II	80199m	^{199}Hg(γ,γ')^{199m}Hg	0.533	TENDL-2023	80199m
^{204}Pb(n,n')^{204m}Pb	0.220	IRDFF-II	82204m	^{204}Pb(γ,γ')^{204m}Pb	0.219	TENDL-2023	102
(n,2n) and (γ,n) reactions on the same target and leading to production of the same isotope							
^{19}F(n,2n)^{18}F	10.986	IRDFF-II	16	^{19}F(γ,n)^{18}F	10.432	IAEA/PD-2019	9018
^{23}Na(n,2n)^{22}Na	12.965	IRDFF-II	16	^{23}Na(γ,n)^{22}Na	12.420	IAEA/PD-2019	11022
^{27}Al(n,2n)^{26}Al	13.546	IRDFF-II	16	^{27}Al(γ,n)^{26}Al	13.058	IAEA/PD-2019	10/5/1
^{46}Ti(n,2n)^{45}Ti	13.479	IRDFF-II	16	^{46}Ti(γ,n)^{45}Ti	13.189	IAEA/PD-2019	22045
^{55}Mn(n,2n)^{54}Mn	10.414	IRDFF-II	16	^{55}Mn(γ,n)^{54}Mn	10.227	IAEA/PD-2019	25054
^{54}Fe(n,2n)^{53}Fe	13.629	IRDFF-II	16	^{54}Fe(γ,n)^{53}Fe	13.378	IAEA/PD-2019	26053
^{59}Co(n,2n)^{58}Co	10.633	IRDFF-II	16	^{59}Co(γ,n)^{58}Co	10.454	IAEA/PD-2019	27058
^{58}Ni(n,2n)^{57}Ni	12.429	IRDFF-II	16	^{58}Ni(γ,n)^{57}Ni	12.216	IAEA/PD-2019	28057
^{63}Cu(n,2n)^{62}Cu	11.038	IRDFF-II	16	^{63}Cu(γ,n)^{62}Cu	10.864	IAEA/PD-2019	29062
^{65}Cu(n,2n)^{64}Cu	10.065	IRDFF-II	16	^{65}Cu(γ,n)^{64}Cu	9.911	IAEA/PD-2019	29064
^{75}As(n,2n)^{74}As	10.383	IRDFF-II	16	^{75}As(γ,n)^{74}As	10.245	IAEA/PD-2019	33074
^{89}Y(n,2n)^{88}Y	11.612	IRDFF-II	16	^{89}Y(γ,n)^{88}Y	11.482	IAEA/PD-2019	4
^{90}Zr(n,2n)^{89}Zr	12.103	IRDFF-II	16	^{90}Zr(γ,n)^{89}Zr	11.968	IAEA/PD-2019	10/5/1
^{93}Nb(n,2n)^{92m}Nb	9.063	IRDFF-II	41092m	^{93}Nb(γ,n)^{92m}Nb	8.966	IAEA/PD-2019	41092m
^{115}In(n,2n)^{114m}In	9.311	IRDFF-II	49114m	^{115}In(γ,)^{115m}In	9.230	IAEA/PD-2019	49114m
^{127}I(n,2n)^{126}I	9.217	IRDFF-II	16	^{127}I(γ,n)^{126}I	9.144	IAEA/PD-2019	53126
^{141}Pr(n,2n)^{140}Pr	9.464	IRDFF-II	16	^{141}Pr(γ,n)^{140}Pr	9.397	IAEA/PD-2019	59140
^{169}Tm(n,2n)^{168}Tm	8.082	IRDFF-II	16	^{169}Tm(γ,n)^{168}Tm	8.034	IAEA/PD-2019	4
^{197}Au(n,2n)^{197}Au	8.114	IRDFF-II	16	^{197}Au(γ,n)^{196}Au	8.072	IAEA/PD-2019	79196
^{209}Bi(n,2n)^{208}Bi	7.496	IRDFF-II	16	^{209}Bi(γ,n)^{208}Bi	7.460	IAEA/PD-2019	83208
^{238}U(n,2n)^{237}U	6.180	IRDFF-II	16	^{238}U(γ,n)^{237}U	6.154	IAEA/PD-2019	92237
(n,3n) and (γ,2n) reactions on the same target and leading to production of the same isotope							
^{59}Co(n,3n)^{57}Co	19.352	IRDFF-II	17	^{59}Co(γ,2n)^{57}Co	19.027	IAEA/PD-2019	16
^{169}Tm(n,3n)^{167}Tm	14.963	IRDFF-II	17	^{169}Tm(γ,2n)^{167}Tm	14.874	IAEA/PD-2019	16
^{209}Bi(n,3n)^{207}Bi	14.416	IRDFF-II[a]	17	^{209}Bi(γ,2n)^{207}Bi	14.347	IAEA/PD-2019	83207
(n,xn) and (γ,(x-1)n) reactions on the ^{209}Bi, where x = 4 – 10, leading to production of the same isotope							
^{209}Bi(n,4n)^{206}Bi	22.553	IRDFF-II[a]	37	^{209}Bi(γ,3n)^{206}Bi	22.444	IAEA/PD-2019	83206
^{209}Bi(n,5n)^{205}Bi	29.622	IRDFF-II[a]	152	^{209}Bi(γ,4n)^{205}Bi	29.479	IAEA/PD-2019	83205
^{209}Bi(n,6n)^{204}Bi	38.152	IRDFF-II[a]	153	^{209}Bi(γ,5n)^{204}Bi	37.969	IAEA/PD-2019	83204
^{209}Bi(n,7n)^{203}Bi	45.380	IRDFF-II[b]	160	^{209}Bi(γ,6n)^{203}Bi	45.162	IAEA/PD-2019	83203
^{209}Bi(n,8n)^{202}Bi	54.277	IRDFF-II[b]	161	^{209}Bi(γ,7n)^{202}Bi	54.017	IAEA/PD-2019	83202
^{209}Bi(n,9n)^{201}Bi	61.710	IRDFF-II[b]	162	^{209}Bi(γ,8n)^{201}Bi	61.414	TENDL-2023	83201
^{209}Bi(n,10n)^{202}Bi	70.870	IRDFF-II[b]	163	^{209}Bi(γ,9n)^{200}Bi	70.529	TENDL-2023	83200

Neutron induced reaction				Gamma induced reaction			
Reaction	Thresh, MeV	Library	MT or ZAP	Reaction	Thresh, MeV	Library	MF/MT /ZAP
(n,np+d) and (γ,p) reactions on the same target and leading to production of the same isotope							
^{29}Si(n,np)^{28}Al	10.461	IRDFF-II	13028	^{29}Si(γ,p)^{28}Al	12.334	IAEA/PD-2019	13028
(n,α) and (γ,h) reactions on the same target and leading to production of the same isotope							
^{27}Al(n,α)^{24}Na	3.249	IRDFF-II	107	^{27}Al(γ,h)^{24}Na	23.710	IAEA/PD-2019	10/2003
^{51}V(n,α)^{48}Sc	2.095	IRDFF-II	107	^{51}V(γ,h)^{48}Sc	22.631	IAEA/PD-2019	21048
^{54}Fe(n,α)^{51}Cr	0.000	IRDFF-II	107	^{54}Fe(γ,h)^{51}Cr	19.734	IAEA/PD-2019	24051
^{59}Co(n,α)^{56}Mn	0.000	IRDFF-II	107	^{59}Co(γ,h)^{56}Mn	20.249	IAEA/PD-2019	106
^{63}Cu(n,α)^{60}Co	0.000	IRDFF-II	107	^{63}Cu(γ,h)^{60}Co	18.861	IAEA/PD-2019	27060

Note: a) Cross sections for ^{209}Bi(n,xn), x = 2 – 6, are included in IRDFF-II up to incident neutron energy 400 MeV.
b) Cross sections for ^{209}Bi(n,xn), x = 7 – 10, are not included in IRDFF-II yet. They were taken from the preliminary evaluation of V. Pronayev for ^{209}Bi(n,xn), x = 7 – 10, up to incident neutron energy 100 MeV [5].

All competing reactions are arranged in several sub-groups in accordance with their type: (n,f) and (γ,f), (n,n') and (γ,γ'), (n,2n) and (γ,n), (n,3n) and (γ,2n), (n,xn) and (γ,(x-1)n) where multiplicity x = 4 - 10, (n,np+d) and (γ,p), (n,α) and (γ,h). The sub-groups are ordered according to the increase of kinematic thresholds, and within the sub-groups by element charge number Z. The kinematic thresholds for the neutron- and gamma-induced reactions were calculated by the own developed code *SKNMT* that uses the nuclei isotope masses from the mass evaluation database AME2020 [6].

The cross sections for neutron induced reactions were taken from the dedicated dosimetry library IRDFF-II (the latest release of January 2020) [1]. It contains in total 93 reactions for the mono-isotopes and 26 for natural elements as targets. The incident neutron energy range extends from threshold up to energy 60 MeV. The exception is the cross sections for reactions (n,xn) with the neutron multiplicity x = 2 - 6, on ^{209}Bi, which have the high energy cut-off 400 MeV.

The cross sections for the extreme high threshold reactions ^{209}Bi(n,xn), x = 7 – 10, are not included in IRDFF-II yet. In the present work we used for these reactions the preliminary evaluation of V. Pronyaev which provides the cross sections and uncertainties up to incident neutron energy 100 MeV [5]. Fig. 2.1 depicts the experimental data found in database EXFOR [7] in comparison with the V. Pronyaev [5] and TENDL-2023 [4] evaluations. It shows that existing measurements [8], [9] and [10] are extremely scarce and controversial, the spread between two evaluations is unacceptably large. In general, V. Pronyaev's evaluation seems to be closer to the experiment and was therefore selected for our present assessments. To improve the status of the high threshold neutron dosimetry reactions, the call for measurements and evaluation was formulated in the Nuclear data high priority request list (HPRL) [11].

For retrieving the specific dosimetry reaction cross sections, we used the proper MT numbers accepted in the IRDFF-II library [1] (it has to be noticed that most IRDFF-II point-wise cross sections are stored in file MF = 3). In several cases, the combination ZAP = 1000*Z + A, where Z and A are the charge and mass numbers of the residual isotope, is a unique identification of the dosimetry reaction (in that case the cross sections are stored in file MF = 10). If the excitation and decay of the metastable state of the residual radionuclide serve as a neutron dosimeter, then the letter "m" is added to ZAP. The proper information is given in Table 2.1 for each considered reaction.

The cross sections for gamma induced reactions were taken from the dedicated photonuclear library IAEA/PD-2019.2 (the latest update was released on October 31, 2022) [3]. In total, it contains the evaluated photonuclear cross sections for 219 isotopes, the highest gamma energies extend mostly up to 200 MeV. For the unique identification of the required photonuclear reaction, the final product identification ZAP is often sufficient. In some cases, the combination of the file (MF) and reaction (MT) numbers is necessary [3], [12], see Table 2.1.

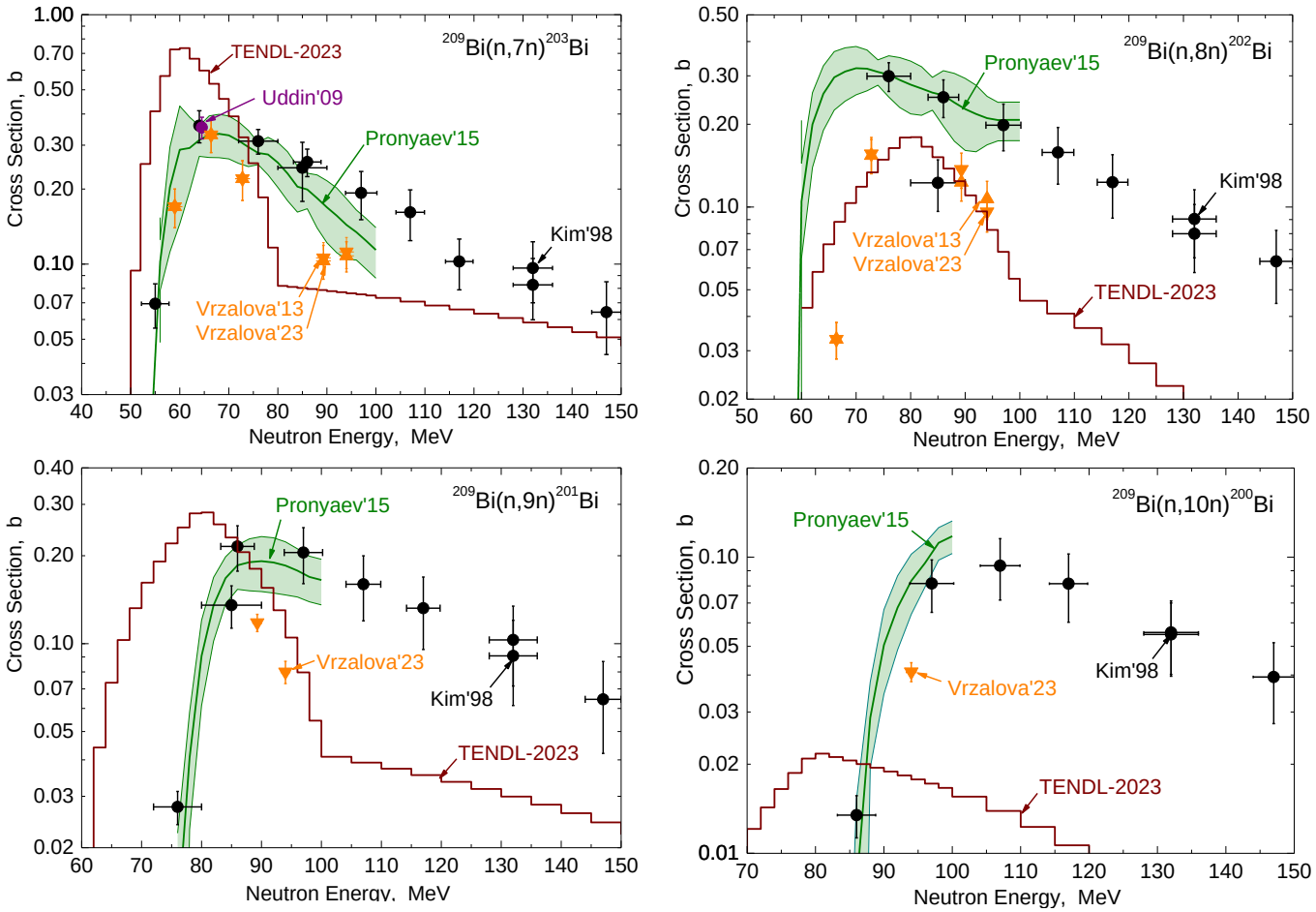

FIG. 2.1. Cross sections for the neutron induced reactions ^{209}Bi(n,xn)$^{209-x+1}$Bi with the neutron multiplicity x = 7 – 10: existing measurements [8] - [10] (symbols) and evaluations from V. Pronyaev (green curve with corridor of uncertainty) [5] and from TENDL-2023 (brown histogram) [4].

Since IAEA/PD-2019.2 has no evaluations for ^{113}In, ^{199}Hg, ^{204}Pb and ^{241}Am, the corresponding cross sections were taken from the gamma sub-library of TENDL-2023 [4] (namely, the library option that includes all explicit channels up to 200 MeV). The photonuclear cross section for the reaction ^{103}Rh(γ,γ') ^{103m}Rh was also taken from TENDL-2023, since the IAEA/PD-2019.2 cross section only starts above 5 MeV which is not acceptable for the reaction with low kinematic threshold 0.040 MeV (Table 2.1).

For the reaction ^{90}Zr(γ,1n)^{89}Zr from IAEA/PD-2019.2 we found that the cross section of ^{90}Zr(γ,x)^{89}Zr leading to the residual ^{89}Zr (final product identification ZAP = 40089) has a non-zero value below the kinematic threshold 11.968 MeV, Fig. 2.2. This results in a substantially wrong overestimation of the spectrum averaged cross sections, since the gamma spectra from considered radiation sources decrease exponentially, Fig. 2.2. To avoid this defect of IAEA/PD-2019.2, we used the ^{90}Zr(γ,1n)X cross section (MF/MT/ZAP = 10/5/1). As can be seen, the latter agrees with the needed ^{90}Zr(γ,x)^{89}Z cross section in the energy range between the thresholds for (γ,1n) and (γ,2n). At an energy above 21.3 MeV, the ^{90}Zr(γ,1n)X cross section obviously includes the double value of the ^{90}Zr(γ,2n)^{88}Zr cross section (i.e., the neutron emission). Since at such high energies the gamma spectrum exponentially falls, the impact on γ-SACS is expected to be rather small with little impact on the accuracy sufficient for the present assessments.

A similar wrong energy dependence was observed for the cross section ^{27}Al(γ,x)^{24}Na from IAEA/PD-2019.2. Fig. 2.3 shows that the cross section for the production of ^{24}Na (identification MF/MT/MT = 10/5/11024) has a non-physical bump below the reaction kinematic threshold 23.710 MeV. To overcome this problem, the helion emission cross section ^{27}Al(γ,x)^{3}He (MF/MT/MT = 10/5/2003) was selected in the present calculations.

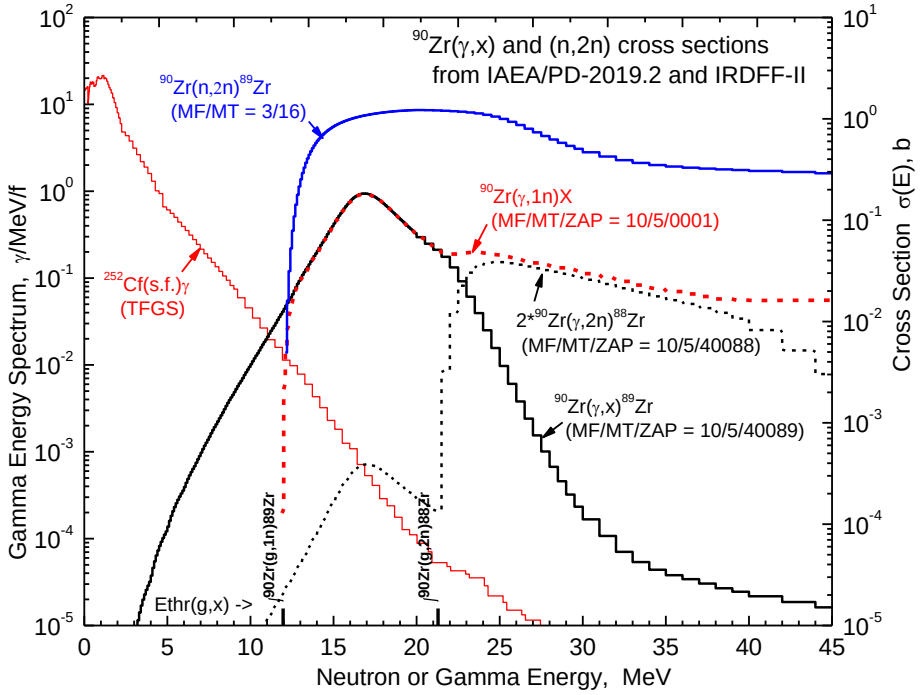

FIG. 2.2. (Right Axis) The neutron (IRDFF-II) and gamma (IAEA/PD-2019.2) induced cross sections for ^{90}Zr (extracted with indicated MF/MT/ZAP): ^{90}Zr(n,2n)^{89}Zr - blue histogram; ^{90}Zr(γ,x)^{89}Zr – black, ^{90}Zr(γ,x)^{89}Zr – dashed red, double neutron emission ^{90}Zr(γ,2n) – dashed black.
(Left axis) The absolute total energy emission spectra of γ-rays from ^{252}Cf(s.f.) (thin red histogram), for more details see Section 3.

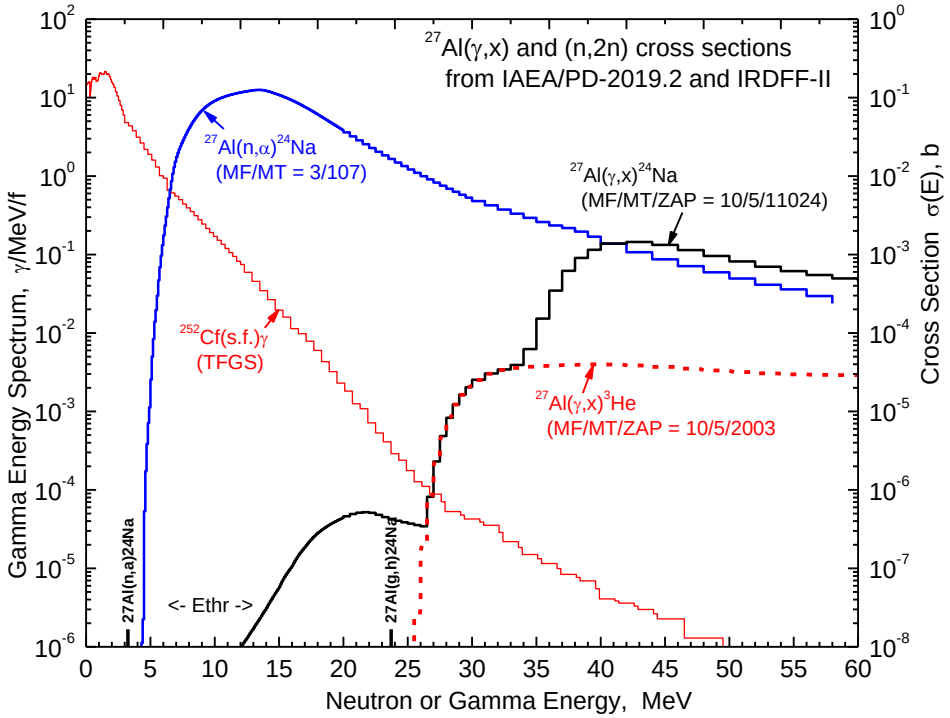

FIG. 2.3. (Right Axis) The neutron (IRDFF-II) and gamma (IAEA/PD-2019.2) induced cross sections (extracted with indicated MF/MT/ZAP) for ^{27}Al: ^{27}Al(n,α)^{24}Na – blue histogram; ^{27}Al(γ,x)^{24}Na – black, ^{27}Al(γ,x)^{3}He – dashed red.
(Left axis) The absolute total energy emission spectra of γ-rays from ^{252}Cf(s.f.) (thin red histogram), for more details see Section 3.

The neutron induced (IRDFF-II) and photonuclear (IAEA/PD-2019.2 or TENDL-2023) libraries were processed in the fine multigroup representation by the PREPRO2023 code [13]. The 765 group structure was selected, which consists of SAND-II structure (up to 20 MeV), plus 2 MeV energy bins up to 60 MeV, plus 2 MeV bins up to 100 MeV and plus 5 MeV bins up to 200 MeV. The proper built-in group structure was invoked in the GROPIE module of PREPRO2023.

It is worth noticing that the SAND-II 725 group structure up to 60 MeV is traditionally used for the IRDFF-II representation up to 60 MeV, which is the high energy end for most neutron dosimetry reactions in this library [1]. The necessity of the IRDFF-II group-wise cross section extension from 60 MeV to 200 MeV in the present work was dictated by high threshold reactions ^{209}Bi(n,xn), x = 2 – 6, which are part of IRDFF-II but have the high neutron energy limit 400 MeV. The eventually selected 200 MeV end-point for grouped neutron and gamma cross sections in the present calculations is limited by the achievable extension of the ^{252}Cf(s.f.) and ^{235}U(n_{th},f) radiation spectra towards the high energies, see next Section.

3. Neutron and γ-ray energy spectra from ^{252}Cf(s.f.) and ^{235}U(n_{th},f)

This first two sub-sections review the status of the neutron and gamma energy spectra and averaged multiplicities for the ^{252}Cf(s.f.) and ^{235}U(n_{th},f) sources of mixed radiations. The basic characteristics of the gamma and neutron emission and references from which the numerical data were taken, are summarised in Table 3.1. It shows that the prompt neutron and gamma spectra have the high energy cut-off around 20 – 30 MeV.

The last sub-section considers the extrapolation of the reference ^{252}Cf(s.f.) and ^{235}U(n_{th},f) prompt neutron and gamma spectra to higher energies, i.e. to 100 or 200 MeV. This opens the possibility to assess the contribution of the photonuclear reactions to the residual production in comparison with those neutron dosimetry reactions that have kinematic thresholds E_{thr} in the range from 20 to 100 MeV.

TABLE 3.1. Main parameters of the neutron and γ-ray radiations from spontaneous fission of ^{252}Cf and thermal neutron induced fission of ^{235}U.
(*The average neutron (ν) and gamma (M_γ) multiplicities are normalized per fission event (f). The spectrum average energies (ε) were calculated from the referenced energy spectra. The data origin is given.)*

Emission mode	Neutrons			Gammas		
	Multiplicity ν, n/f	Spectrum Range MeV	ε_n MeV	Multiplicity M_γ, γ/f	Spectrum Range MeV	ε_γ MeV
	^{252}Cf spontaneous fission: P_{sf} = (3.086 ± 0.008)%, $T_{1/2}$ = (85.76 ± 0.23) y					
Prompt	3.7590 ± 0.048 [17]	0.00001 – 30.0 [15]	2.122	9.194 [21]	0.1 – 20.0 [21]	0.813
Delayed	0.0086 ± 0.010 [19],[17]	0.0 – 3.0 [17]	0.477	10.3 [22],[23]	0.0 - 2.0 [22],[23]	0.774
Total	**3.7676 ± 0.016** [20],[17]			**19.49** [a]		
	^{235}U thermal neutron induced fission: cross section σ_f = 587.3 ± 1.4 b [1]					
Prompt	2.425 ± 0.011 [15]	0.10 – 30.0 [15],[17]	2.000	8.57905 [17]	0.01 – 21.35 [17]	0.849
Delayed	0.01585 ± 0.00071 [17]	0.0 – 3.0 [17]	0.509	-	-	
Total	**2.44085 ± 0.011** [a]					

Note: a) arithmetic sum of prompt and delayed multiplicities.

3.1. Known information about ^{252}Cf(s.f.) neutron and gamma energy spectra and multiplicities

The prompt fission neutron spectrum (PFNS) from spontaneous fission of ^{252}Cf was measured in several experiments. Both the energy differential data and the neutron averaged cross sections were used by W. Mannhart in his non-model evaluation [14]. The evaluated ^{252}Cf(s.f.) PFNS was accepted as a standard spectrum in the IAEA project "Neutron Data Standards" [15], [16]. Its uncertainty amounts to 1 – 12% in the emission neutron energy range 0.1 – 15 MeV. For our calculations we took the numerical PFNS data in the 725 group presentation from the database IRDFF-II [1]. The prompt neutron multiplicity, i.e. the number of prompt neutrons per spontaneous ^{252}Cf fission ν_p = 3.7590 ± 0.0048 were taken from Standards [15].

The ^{252}Cf(s.f.) delayed fission neutron spectrum (DFNS) is available in library ENDF/B-VIII.0 [17] and presented there for 6 delayed time groups in the section MF/MT = 5/455. The DFGS, summed over the time groups, was derived with the retrieving system JANIS of the NEA Databank [18]. The delayed neutron multiplicity ν_d = 0.0086 ± 0.010 was taken from ENDF/BVIII.0 [17], which in turn refers to the evaluation of T. England [20] as a primary resource.

Similar to PFNS, the ^{252}Cf(s.f.) prompt fission γ-ray spectrum (PFGS) was also intensively measured in many labs during the last several decades. Based on these experimental data, PFGS was recently evaluated and proposed as a reference in the energy range 0.1 to 20 MeV [21]. This evaluation also provided the prompt gamma multiplicity M_γ = 9.194 γ/f by integration of PFGS in the evaluated range and extrapolation below 0.1 MeV, see Table 3.1.

For the ^{252}Cf(s.f.) delayed fission gamma spectrum (DFGS), it was shown [21] that existing measurements, theoretical models or contemporary evaluations are not sufficient for the delayed gamma spectrum evaluation and recommendation. In present calculations we used an evaluation carried out by Stoddard in 1965 [22], [23], which is rather old but the only existing one. He also provided the delayed gamma multiplicity M_γ = 10.3 γ/f.

Fig. 3.1 shows the prompt neutron and γ-ray energy absolute energy differential spectra (number of neutrons or gammas per energy unit and fission event *f*) from ^{252}Cf(s.f.).

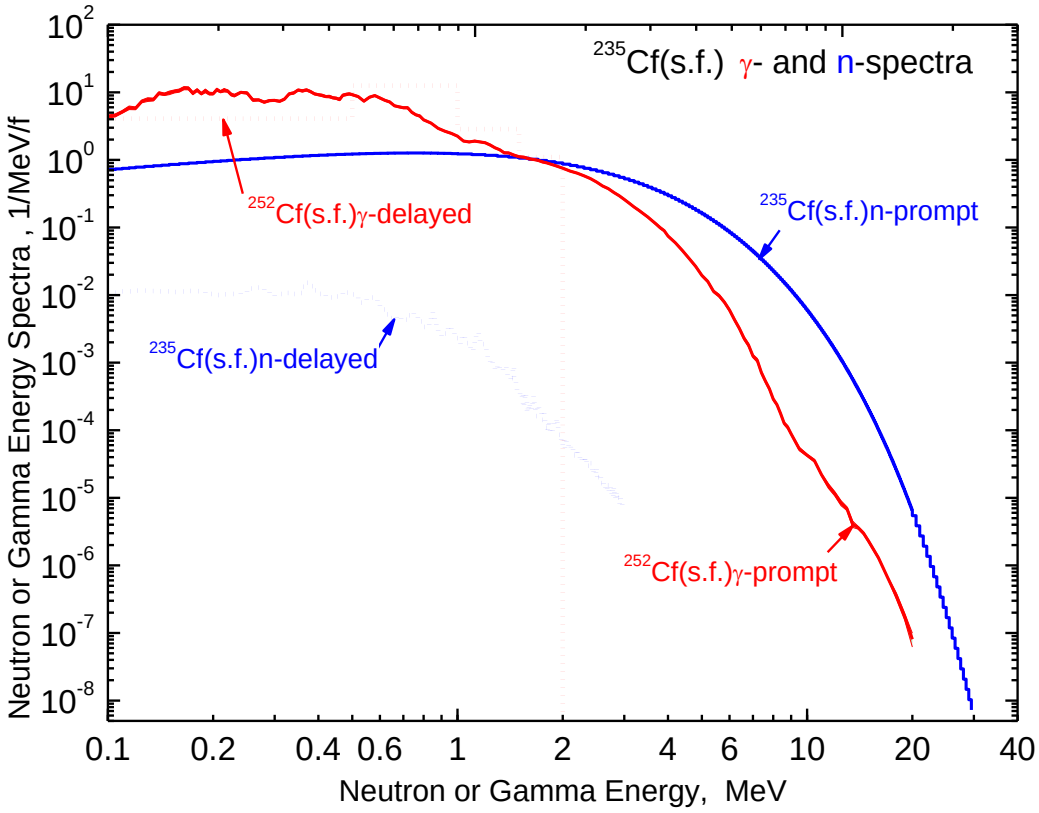

FIG. 3.1. The absolute energy differential spectra of the prompt and delayed γ-rays and neutrons from ^{252}Cf(s.f.) available in the most recent evaluations: PFNS and DFNS - from IAEA Standards [15] and ENDF/B-VIII.0 [17]; PFGS – Simakov [21], DFGS - Stoddard [22], [23].

3.2. Known information about $^{235}U(n_{th},f)$ neutron and gamma energy spectra and multiplicities

The prompt fission neutron spectrum (PFNS) from the thermal neutron induced fission of ^{235}U was also rather well investigated, see [24], [25]. $^{235}U(n_{th},f)$ PFNS is included as a reference spectrum in the IAEA Standards [15], [16] as well as in the ENDF/B-VIII.0 [17] and IRDFF-II [1] libraries. We derived the PFNS and covariance numerical values from section MT = 18 of files MF = 5 and MF = 35 of ENDF/B-VIII.0, respectively. The prompt neutron multiplicity, i.e. the number of prompt neutrons per $^{235}U(n_{th},f)$ fission event, $\nu_p = 2.425 \pm 0.011$ n/f was taken from Standards [15], [16] (this value is slightly higher than the value $\nu_p = 2.414$ n/f given in ENDF/VIII.0, section MT = 456 of file MF = 1).

The $^{235}U(n_{th},f)$ delayed fission neutron energy spectra (DFNS) were derived from ENDF/B-VIII.0 [17] from section MF/MT = 5/455 by means of JANIS. The delayed neutron multiplicity and its uncertainty $\nu_d = 0.01585 \pm 0.00071$ n/f were taken from sections MF/MT = 1/455 and MF/MT = 31/455 of ENDF/VIII.0 [17].

The $^{235}U(n_{th},f)$ prompt γ-ray spectrum (PFGS) at thermal neutron energy was extracted for our calculations from section MT = 18 of file MF = 15 of ENDF/B-VIII.0 [17] (the PFGS covariances are not presented in this library). This evaluation was based on the statistical model calculations [26] and existing measurements with a preference for the experimental data of A. Oberstedt et al. [27]. The evaluators in their recent paper [28] confirmed that $^{35}U(n_{th},f)$ PFGS and multiplicity as given in ENDF/B-VIII.0 continue to be the best ones regarding even the new published experimental data. The prompt γ-ray multiplicity $M\gamma = 8.57905$ γ/f for $^{235}U(n_{th},f)$ was also extracted from the ENDF/B-VIII.0 library, from section MT = 18 and file MF = 12. This value is based on DFGS, measured above 0.1 MeV but calculated below 0.1 MeV, and on the measured γ-ray multiplicity distributions.

The information about the $^{235}U(n_{th},f)$ delayed fission gamma energy spectrum (DFGS) and γ-ray multiplicity seems to be not available in the contemporary evaluated nuclear data libraries.

Fig. 3.2 shows the prompt neutron and γ-ray energy absolute energy differential spectra (number of neutrons or gammas per energy unit and fission event *f*) from $^{235}U(n_{th},f)$.

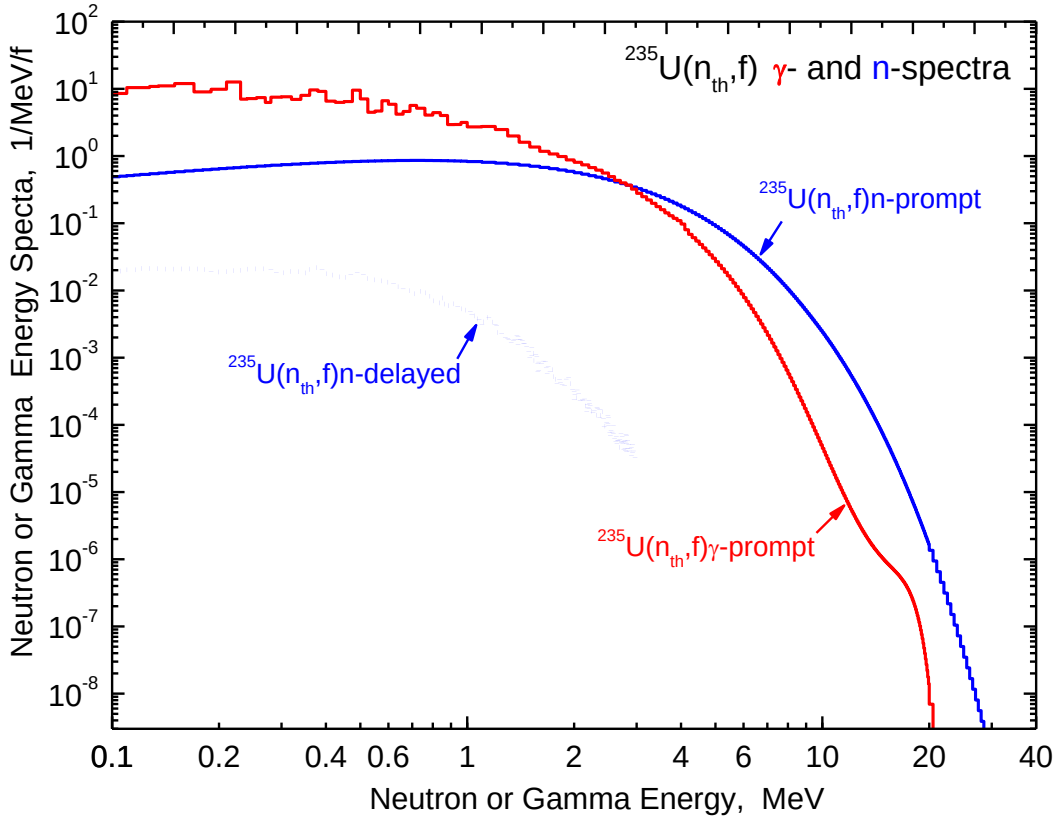

FIG. 3.2. The absolute energy differential spectra of the prompt and delayed γ-rays and neutrons from $^{235}U(n_{th},f)$ available in the most recent evaluations: PFNS, DFNS – from IAEA Standards [15] or ENDF/B-VIII.0 [17]; PFGS – ENDF/B-VIII.0 [17].

3.3. Extension of ^{252}Cf(s.f.) and ^{235}U(nth,f) neutron and gamma spectra above 20 - 30 MeV and their processing

Figs 3.3 and 3.4 depict the known information about the prompt and delay neutron and γ-ray energy spectra from ^{252}Cf(s.f.) and ^{235}U(n_{th},f). They show that the delayed radiation energy spectra are limited to around 3 MeV, the prompt ones extend up to 20 or 30 MeV. Additionally, these Figures present the cross sections for several high energy neutron dosimetry reactions ^{209}Bi(n,xn) with multiplicity x = 2, 4 and 6 (Fig. 3.3) and corresponding competing photonuclear reactions ^{209}Bi(γ,(x-1)n) (Fig. 3.4). As can be seen, if the high energy limit 20 – 30 MeV for PFNS and PFGS is sufficient for accurate estimation of the spectrum averaged cross sections (SACS) for the pair ^{209}Bi(n,2n) and ^{209}Bi(γ,1n), it is too small for reactions producing a larger number of neutrons.

For calculation of SACS and estimation of the (γ,x) impact for all neutron dosimetry reactions included in IRFFF-II, the extension of the prompt energy spectra above 20 - 30 MeV for the ^{252}Cf(s.f.) and ^{235}U(n_{th},f) radiation sources is necessary.

For the neutron spectra there is not any experimental or theoretical information above 30 MeV. We extrapolated PFNS from 30 MeV to 100 MeV employing the exponential law which was fitted to the reference PFNS between 20 and 30 MeV. The resultant prompt fission neutron spectra for the ^{252}Cf(s.f.) and ^{235}U(n_{th},f) sources are depicted in Figs 3.3 and 3.4.

The gamma energy spectra were extrapolated from 20 MeV in the case of ^{252}Cf(s.f.) or from 30 MeV in the case of ^{235}U(n_{th},f) up to 200 MeV, Figs 3.3 – 3.5. As seen, the gamma spectra from these two sources have a similar shape up to 20 – 30 MeV. At higher energies, as it was discussed in the review [21], the most relevant are the measurements of D. Pandit et al. [29] for ^{252}Cf(s.f.)γ and V. Varlachev et al. [30], [31] for ^{235}U(n_{th},f)γ, Fig. 3.5. The recent experiments for ^{235}U(n_{th},f) provided PFGS data only up to 19.5 MeV (H. Makii et al. [32]) or 9.5 MeV (T. Wright et al. [33]). Above 40 – 50 MeV we additionally included gamma spectra originating from the π^0 decay, for more details see [21].

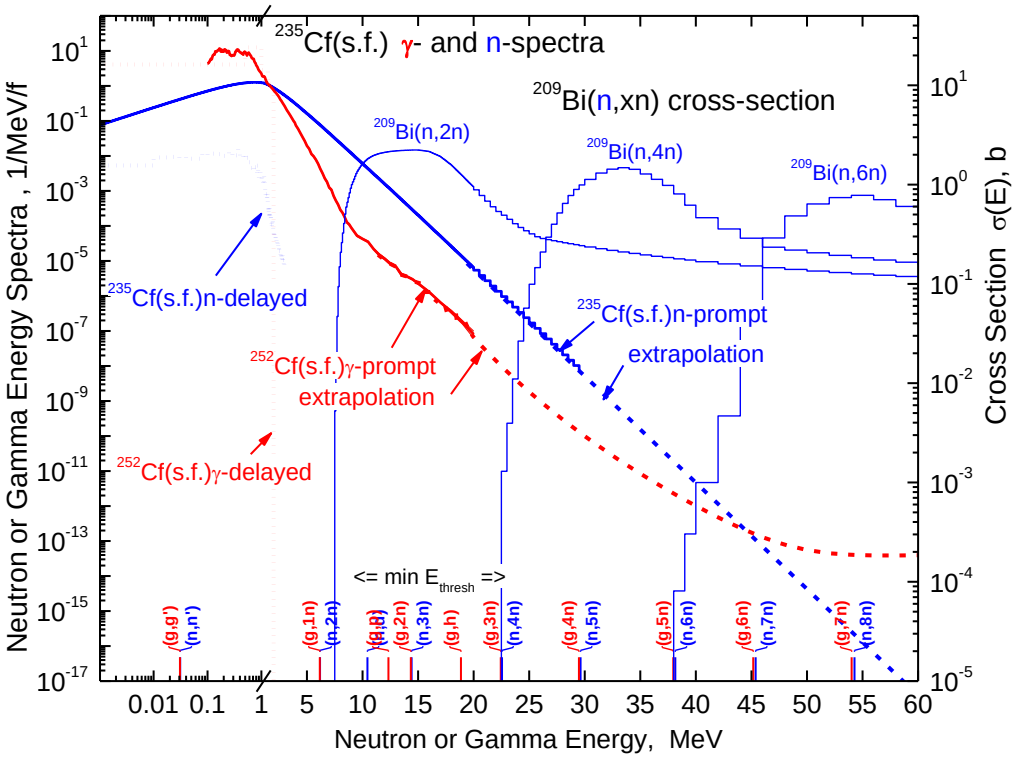

FIG. 3.3. (Left axis) The energy spectra of the neutrons (blue curves) and γ-rays (red) from ^{252}Cf(s.f.) up to energy 60 MeV: PFNS – Standards up to 30 MeV, above – extrapolation; DFNS - ENDF/B-VIII.0; PFGS – evaluation in range 0.1 – 20 MeV [21], above – extrapolation. The minimal kinematic thresholds for the indicated competing reaction pairs are shown above X-axis.
(Right axis) Neutron cross sections from IRDFF-II for reactions: ^{209}Bi(n,2n)^{208}Bi, ^{209}Bi(n,4n)^{206}Bi and ^{209}Bi(n,6n)^{205}Bi (blue histograms).

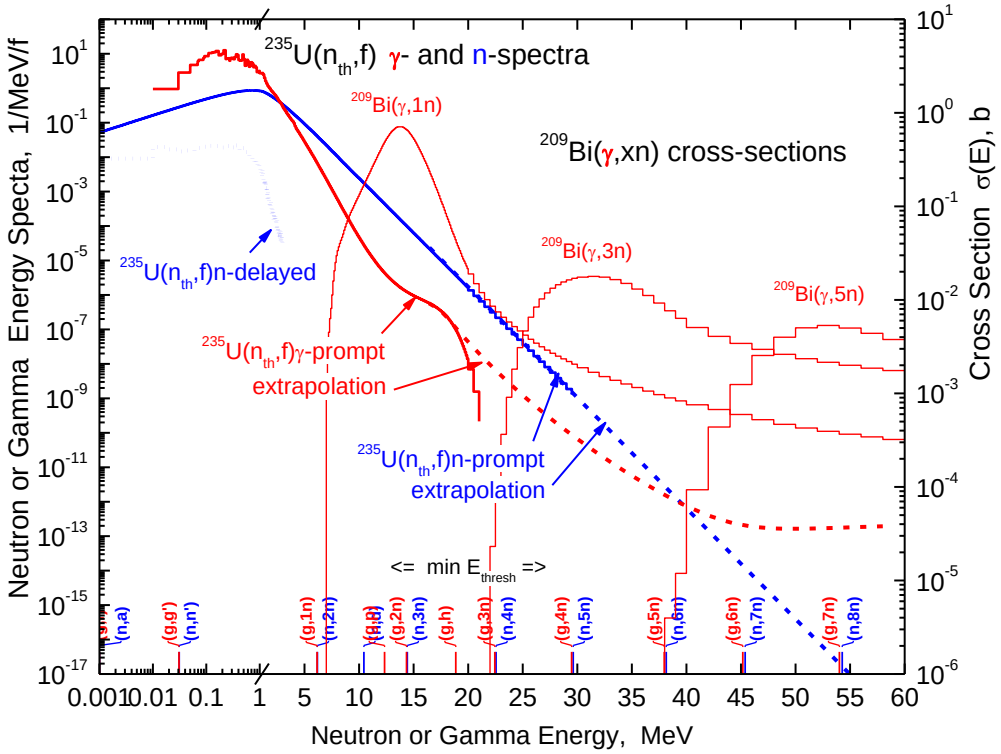

FIG. 3.4. (Left axis) The energy spectra of the neutrons (blue curve) and γ-rays (red) from $^{235}U(n_{th},f)$ up to energy 60 MeV. PFNS – Standards up to 30 MeV, above – extrapolation; DFNS - ENDF/B-VIII.0; PFGS – ENDF/B-VIII.0. The minimal kinematic thresholds for the indicated competing reaction pairs are shown above X-axis.
(Right axis) Gamma cross sections from IAEA/PN-2019.2 for: $^{209}Bi(\gamma,1n)^{208}Bi$, $^{209}Bi(\gamma,3n)^{206}Bi$ and $^{209}Bi(\gamma,5n)^{205}Bi$ (red histograms), which produce the same radioisotope as $^{209}Bi(n,2n)^{208}Bi$, $^{209}Bi(n,4n)^{206}Bi$ and $^{209}Bi(n,6n)^{205}Bi$ (Fig. 3.3).

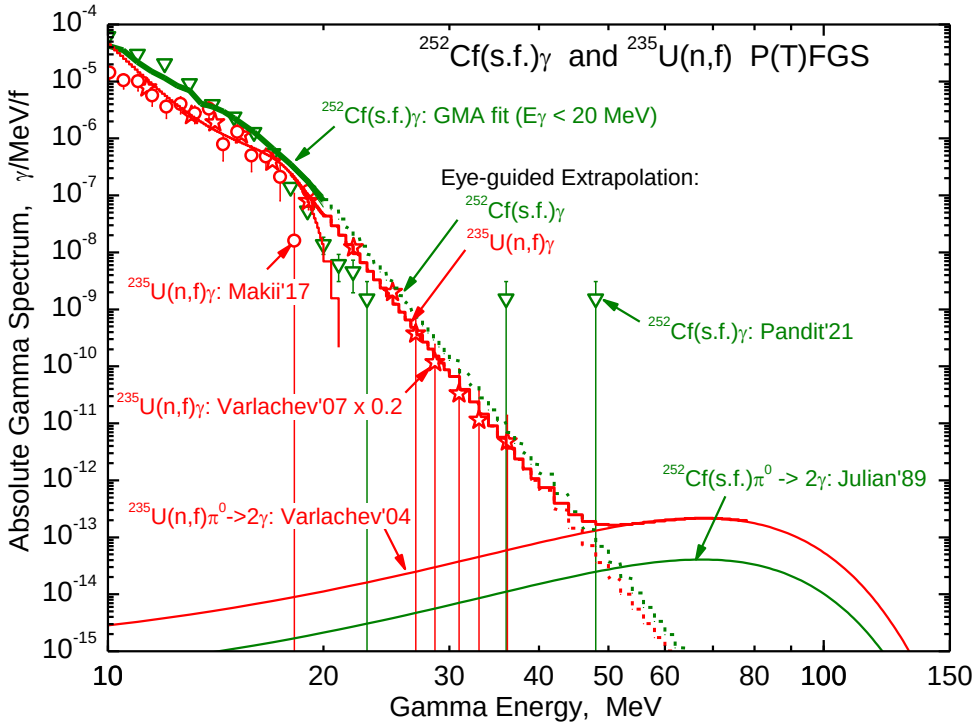

FIG. 3.5. The high energy parts of the prompt γ-rays spectra for $^{252}Cf(s.f.)$ (green curves) and $^{235}U(n_{th},f)$ (red) from 10 to 150 MeV. Symbols: measured data available in EXFOR. Curves: GMA fit up to 20 MeV for $^{252}Cf(s.f.)\gamma$ [21] and ENDF/B-VIII.0 [17] for $^{235}U(n_{th},f)\gamma$ (solid); exponential extrapolation between 20 and 50 MeV (dashed); gamma spectrum following the π^0 decay (solid).

As seen in Figs 3.3 and 3.4, the absolute energy spectra of gammas from both sources ^{252}Cf(s.f.) and ^{235}U(n_{th},f) begin to exceed the neutron spectra above the radiation energy 40 – 45 MeV. Therefore, we may expect that contribution of the high threshold ($E_{thr} \geq 45$ MeV) gamma induced reactions to the residual production will dominate over neutron ones. It is important to underline that change of the PFGS energy shape from exponential decrease to plateau around 45 MeV relies on experimental data which provide only the upper limits, for more details see [21].

The ^{252}Cf(s.f.) and ^{235}U(n_{th},f) neutron and γ-ray spectra were processed into the 765 energy groups up to 200 MeV by PREPRO-2023 [13], i.e. to the same group structure as the neutron and gamma induced reaction cross sections.

It is worth noticing that the addition of the delayed neutron and gamma spectra to the prompt ones results in rather small (less than 1%) changes of the n-SACS and γ-SACS, even for the low threshold reactions such as induced fission or inelastic scattering.

4. Calculation of the neutron and gamma induced SACS and residual production Yields for monoisotopic targets

This Section presents the results of calculations of the neutron- and gamma-induced spectrum average cross sections, n-SACS and γ-SACS, and absolute residual production yields, n-Yield and γ-Yield, which characterize the competition between these two processes in the ^{252}Cf(s.f.) and ^{235}U(n_{th},f) n-γ mixed fields.

n-SACS and γ-SACS were calculated with the help of the RR_UNC code [34]. The (n,x) and (γ,x) cross sections were invoked from the latest version of the dedicated neutron dosimetry library IRDFF-II [1] and photo-nuclear evaluated data libraries IAEA/PD-2019.2 [3] or TENDL-2023 [4] with the help of proper MF/MT/ZAP numbers, see Section 2. The ^{252}Cf(s.f.) and ^{235}U(n_{th},f) neutron and gamma energy spectra were composed from the reference spectra up to 20 or 30 MeV and extrapolation up to 100 – 200 MeV, see Section 3. Both cross sections and energy spectra were processed by PREPRO-2023 [13] into the 765 energy group structure that has high energy cut-off 200 MeV. The normalization of the γ-ray and neutron fluxes as well as corresponding reaction rates was performed per one ^{252}Cf spontaneous fission or ^{235}U thermal neutron induced fission event.

The production of the same reaction observable (radioactive residual isotope or fission event) from the mono-isotopic target was considered for the neutron and gamma induced reactions listed in Table 2.1: (γ,f) and (n,f) for 6 nuclei, (γ,γ') and (n,n') for 6, (γ,n) and (n,2n) for 21, (γ,2n) and (n,3n) for 3, (γ,xn) and (n,(x-1)n) on ^{209}Bi with multiplicity x = 4 - 10 for 7, (γ,p) and (n,np+d) for 1, (γ,^{3}He) and (n,α) for 5. In total – 13 reaction pairs on 49 mono-isotope nuclei.

The relative contribution of the gamma (γ-Fraction) or neutron (n-Fraction) induced reactions to the residual production was calculated according to the following equations:

$$\gamma - Fraction = \frac{\gamma - Yield}{(\gamma - Yield + n - Yield)} = \frac{\gamma - SACS \times M\gamma}{(\gamma - SACS \times M\gamma + n - SACS \times Mn)} \quad (4.1),$$

$$n - Fraction = \frac{n - Yield}{(\gamma - Yield + n - Yield)} = \frac{n - SACS \times Mn}{(\gamma - SACS \times M\gamma + n - SACS \times Mn)} \quad (4.2),$$

where:

- γ-Yield = γ-SACS × Mγ – the absolute gamma induced reaction residual Yield per fission event,
- n-Yield = n-SACS × Mn – the absolute neutron induced reaction residual Yield per fission event,
- Mγ and Mn - the total (prompt +delayed) gamma and neutron Multiplicities per fission event.

Table 4.1 lists the calculated neutron and gamma median energy (E50%), spectrum averaged cross section (SACS), residual production absolute yield (Yield) and relative fraction (Fraction) for the ^{252}Cf(s.f.) and ^{235}U(n_{th},f) γ-n mixed fields. Figs 4.1 and 4.2 show the dependence of the relative contribution (or impact) of the (γ,x) reactions on the total residual production versus the difference between the neutron and gamma median response energies (n-E50% - γ-E50%). As can be seen in these Figures, this representation discovers a certain trend: systematic increase from ≈ 0.002% to ≈ 1% in case of ^{252}Cf(s.f.) source and from ≈ 0.004% up to ≈ 2% in case of ^{235}U(n_{th},f). The maximum is observed for the competing reaction pairs: ^{54}Fe(n,2n)^{53}Fe and ^{54}Fe(γ,n)^{53}Fe, ^{169}Tm(n,3n)^{167}Tm and ^{169}Tm(γ,2n)^{167}Tm.

TABLE 4.1. The γ-ray induced reactions competing with the IRDFF neutron dosimetry reactions in the total neutron or γ-ray fields produced by the ^{252}Cf(s.f.) and ^{235}U(n_{th},f) radiation sources.
(Columns: 50% response energy (E50%), spectrum averaged cross sections (SACS), residual production yield per fission event (Yield) and relative contribution to the total production (Fraction). The photonuclear reactions are highlighted by red font for simplicity of comparison with neutron dosimetry ones.)

Competing Reactions	^{252}Cf(s.f.) mixed n- and γ-fields				^{235}U(n_{th},f) mixed n- and γ-fields			
	E50%, MeV	SACS, mb	Yield, mb/f	Fraction, %	E50%, MeV	SACS, mb	Yield, mb	Fraction, %
(n,f) and (γ,f) reactions leading to the fission and similar Fission Fragments (FF)								
^{230}Th(n,f)FF	2.998	8.225E+01	3.099E+02	99.985	2.866	7.778E+01	1.898E+02	99.964
^{230}Th(γ,f)FF	6.428	2.361E-03	4.602E-02	0.015	6.460	7.890E-03	6.769E-02	0.036
^{235}U(n,f)FF	1.679	1.227E+03	4.623E+03	99.998	1.606	1.226E+03	2.992E+03	99.996
^{235}U(γ,f)FF	6.820	4.754E-03	9.268E-02	0.002	6.764	1.490E-02	1.278E-01	0.004
^{238}U(n,f)FF	2.761	3.175E+02	1.196E+03	99.995	2.659	3.043E+02	7.427E+02	99.988
^{238}U(γ,f)FF	6.482	3.196E-03	6.230E-02	0.005	6.513	1.022E-02	8.771E-02	0.012
^{237}Np(n,f)FF	2.038	1.352E+03	5.093E+03	99.997	1.960	1.336E+03	3.261E+03	99.993
^{237}Np(γ,f)FF	6.454	8.014E-03	1.562E-01	0.003	6.506	2.615E-02	2.244E-01	0.007
^{239}Pu(n,f)FF	1.752	1.796E+03	6.766E+03	99.998	1.681	1.792E+03	4.374E+03	99.996
^{239}Pu(γ,f)FF	6.489	6.836E-03	1.333E-01	0.002	6.510	2.176E-02	1.867E-01	0.004
^{241}Am(n,f)FF	2.215	1.385E+03	5.218E+03	99.996	2.136	1.361E+03	3.322E+03	99.992
^{241}Am(γ,f)FF	6.393	9.700E-03	1.891E-01	0.004	6.427	3.106E-02	2.664E-01	0.008
(n,n') and (γ,γ') reactions on the same target and leading to production of the same isotope								
^{93}Nb(n,n')^{93m}Nb	2.675	1.445E+02	5.443E+02	99.998	2.587	1.403E+02	3.425E+02	99.996
^{93}Nb(γ,γ')^{93m}Nb	3.454	5.667E-04	1.105E-02	0.002	3.753	1.479E-03	1.269E-02	0.004
^{103}Rh(n,n')^{103m}Rh	2.363	7.188E+02	2.708E+03	99.993	2.263	7.033E+02	1.717E+03	99.989
^{103}Rh(γ,γ')^{103m}Rh	3.578	9.458E-03	1.844E-01	0.007	3.854	2.214E-02	1.900E-01	0.011
^{113}In(n,n')^{113m}In	2.723	1.562E+02	5.883E+02	99.996	2.650	1.513E+02	3.692E+02	99.992
^{113}In(γ,γ')^{113m}In	3.578	1.315E-03	2.564E-02	0.004	3.854	3.490E-03	2.994E-02	0.008
^{115}In(n,n')^{115m}In	2.666	1.883E+02	7.096E+02	99.992	2.588	1.828E+02	4.461E+02	99.984
^{115}In(γ,γ')^{115m}In	3.587	2.987E-03	5.823E-02	0.008	3.881	8.104E-03	6.953E-02	0.016
^{199}Hg(n,n')^{199m}Hg	3.089	2.922E+02	1.101E+03	99.999	2.970	2.786E+02	6.799E+02	99.999
^{199}Hg(γ,γ')^{199m}Hg	3.587	3.062E-04	5.968E-03	0.001	3.881	7.864E-04	6.747E-03	0.001
^{204}Pb(n,n')^{204m}Pb	5.038	2.002E+01	7.541E+01	99.308	4.839	1.725E+01	4.210E+01	98.531
^{2043}Pb(γ,γ')^{204m}Pb	3.851	2.696E-02	5.256E-01	0.692	4.105	7.319E-02	6.279E-01	1.469
(n,2n) and (γ,n) reactions leading to the same residual								
^{19}F(n,2n)^{18}F	14.048	1.598E-02	6.019E-02	99.842	13.911	8.061E-03	1.968E-02	99.761
^{19}F(γ,n)^{18}F	12.313	4.871E-06	9.495E-05	0.158	12.184	5.491E-06	4.711E-05	0.239
^{23}Na(n,2n)^{22}Na	15.586	8.356E-03	3.148E-02	99.885	15.483	3.934E-03	9.601E-03	99.815
^{23}Na(γ,n)^{22}Na	16.508	1.853E-06	3.613E-05	0.115	16.949	2.075E-06	1.780E-05	0.185
^{27}Al(n,2n)^{26}Al	16.140	7.511E-03	2.830E-02	99.918	16.030	3.459E-03	8.443E-03	99.853
^{27}Al(γ,n)^{26}Al	16.508	1.191E-06	2.322E-05	0.082	16.949	1.453E-06	1.246E-05	0.147
^{46}Ti(n,2n)^{45}Ti	16.107	1.225E-02	4.614E-02	99.716	16.005	5.648E-03	1.379E-02	99.556
^{46}Ti(γ,n)^{45}Ti	13.742	6.750E-06	1.316E-04	0.284	13.565	7.170E-06	6.151E-05	0.444
^{55}Mn(n,2n)^{54}Mn	12.915	4.630E-01	1.745E+00	99.965	12.796	2.469E-01	6.025E-01	99.949
^{55}Mn(γ,n)^{54}Mn	13.742	3.122E-05	6.086E-04	0.035	13.565	3.565E-05	3.058E-04	0.051
^{54}Fe(n,2n)^{53}Fe	16.593	3.559E-03	1.341E-02	98.928	16.494	1.614E-03	3.939E-03	98.155
^{54}Fe(γ,n)^{53}Fe	16.042	7.451E-06	1.453E-04	1.072	16.504	8.631E-06	7.405E-05	1.845
^{59}Co(n,2n)^{58}Co	13.088	3.993E-01	1.504E+00	99.959	12.974	2.108E-01	5.145E-01	99.941
^{59}Co(γ,n)^{58}Co	14.367	3.143E-05	6.127E-04	0.041	14.450	3.562E-05	3.056E-04	0.059
^{58}Ni(n,2n)^{57}Ni	14.980	8.441E-03	3.180E-02	99.534	14.879	4.077E-03	9.952E-03	99.304
^{58}Ni(γ,n)^{57}Ni	14.889	7.634E-06	1.488E-04	0.466	15.389	8.126E-06	6.972E-05	0.696
^{63}Cu(n,2n)^{62}Cu	13.838	1.945E-01	7.326E-01	99.884	13.721	9.898E-02	2.416E-01	99.836
^{63}Cu(γ,n)^{62}Cu	13.983	4.364E-05	8.507E-04	0.116	14.019	4.640E-05	3.981E-04	0.164
^{65}Cu(n,2n)^{64}Cu	12.678	6.398E-01	2.411E+00	99.938	12.555	3.452E-01	8.425E-01	99.905
^{65}Cu(γ,n)^{64}Cu	12.589	7.697E-05	1.500E-03	0.062	11.964	9.370E-05	8.038E-04	0.095
^{75}As(n,2n)^{74}As	12.913	6.073E-01	2.288E+00	99.913	12.797	3.234E-01	7.895E-01	99.875
^{75}As(γ,n)^{74}As	13.035	1.017E-04	1.983E-03	0.087	12.651	1.156E-04	9.915E-04	0.125

^{89}Y(n,2n)^{88}Y	13.899	3.384E-01	1.275E+00	99.903	13.797	1.716E-01	4.188E-01	99.862
^{89}Y(γ,n)^{88}Y	15.029	6.344E-05	1.237E-03	0.097	15.357	6.730E-05	5.774E-04	0.138
^{90}Zr(n,2n)^{89}Zr	14.420	2.131E-01	8.028E-01	99.874	14.320	1.054E-01	2.572E-01	99.816
^{90}Zr(γ,n)^{89}Zr	15.106	5.176E-05	1.009E-03	0.126	15.478	5.532E-05	4.746E-04	0.184
^{93}Nb(n,2n)^{92m}Nb	11.328	7.739E-01	2.916E+00	99.950	11.210	4.489E-01	1.096E+00	99.917
^{93}Nb(γ,n)^{92m}Nb	12.663	7.419E-05	1.446E-03	0.050	11.283	1.061E-04	9.102E-04	0.083
^{115}In(n,2n)^{114m}In	11.807	1.597E+00	6.018E+00	99.931	11.681	9.031E-01	2.204E+00	99.885
^{115}In(γ,n)^{115m}In	12.257	2.124E-04	4.141E-03	0.069	11.232	2.946E-04	2.527E-03	0.115
^{127}I(n,2n)^{126}I	11.579	2.060E+00	7.762E+00	99.931	11.459	1.178E+00	2.876E+00	99.894
^{127}I(γ,n)^{126}I	12.498	2.766E-04	5.392E-03	0.069	11.594	3.558E-04	3.052E-03	0.106
^{141}Pr(n,2n)^{140}Pr	11.845	1.947E+00	7.334E+00	99.901	11.725	1.097E+00	2.677E+00	99.839
^{141}Pr(γ,2n)^{140}Pr	12.276	3.723E-04	7.257E-03	0.099	11.212	5.042E-04	4.326E-03	0.161
^{169}Tm(n,2n)^{168}Tm	10.382	6.130E+00	2.310E+01	99.928	10.265	3.743E+00	9.137E+00	99.837
^{169}Tm(γ,n)^{168}Tm	11.059	8.557E-04	1.668E-02	0.072	9.724	1.744E-03	1.496E-02	0.163
^{197}Au(n,2n)^{197}Au	10.542	5.411E+00	2.039E+01	99.922	10.414	3.275E+00	7.994E+00	99.847
^{197}Au(γ,n)^{196}Au	11.567	8.210E-04	1.600E-02	0.078	10.250	1.425E-03	1.222E-02	0.153
^{209}Bi(n,2n)^{208}Bi	9.866	9.817E+00	3.699E+01	99.885	9.744	6.190E+00	1.511E+01	99.680
^{209}Bi(γ,n)^{208}Bi	10.142	2.180E-03	4.250E-02	0.115	8.756	5.647E-03	4.844E-02	0.320
^{238}U(n,2n)^{237}U	8.208	2.068E+01	7.790E+01	99.889	8.087	1.451E+01	3.541E+01	99.637
^{238}U(γ,n)^{237}U	8.115	4.444E-03	8.662E-02	0.111	7.826	1.504E-02	1.290E-01	0.363
(n,3n) and (γ,2n) reactions on the same target and leading to production of the same isotope								
^{59}Co(n,3n)^{57}Co	22.385	8.492E-05	3.199E-04	99.426	22.236	3.446E-05	8.410E-05	98.588
^{59}Co(γ,2n)^{57}Co	20.850	9.468E-08	1.846E-06	0.574	20.900	1.404E-07	1.204E-06	1.412
^{169}Tm(n,3n)^{167}Tm	18.439	1.403E-02	5.285E-02	99.400	18.384	6.011E-03	1.467E-02	98.769
^{169}Tm(γ,2n)^{167}Tm	16.506	1.637E-05	3.192E-04	0.600	16.809	2.131E-05	1.828E-04	1.231
^{209}Bi(n,3n)^{208}Bi	18.167	1.821E-02	6.862E-02	99.638	18.092	7.868E-03	1.920E-02	99.291
^{209}Bi(γ,2n)^{208}Bi	16.506	1.278E-05	2.492E-04	0.362	16.809	1.599E-05	1.371E-04	0.709
(n,xn) and (γ,(x-1)n) reactions on the ^{209}Bi, where x = 4 – 10, leading to production of the same isotope								
^{209}Bi(n,4n)^{206}Bi	26.906	2.226E-05	8.387E-05	99.954	26.733	7.748E-06	1.891E-05	99.861
^{209}Bi(γ,3n)^{206}Bi	26.270	2.000E-09	3.899E-08	0.046	26.272	3.068E-09	2.632E-08	0.139
^{209}Bi(n,5n)^{205}Bi	37.772	1.269E-08	4.781E-08	99.442	37.582	2.838E-09	6.926E-09	97.000
^{209}Bi(γ,4n)^{205}Bi	35.624	1.376E-11	2.682E-10	0.558	36.381	2.497E-11	2.142E-10	3.000
^{209}Bi(n,6n)^{204}Bi	46.083	1.829E-11	6.892E-11	91.887	45.761	2.829E-12	6.904E-12	23.821
^{209}Bi(γ,5n)^{204}Bi	54.478	3.122E-13	6.086E-12	8.113	59.228	2.574E-12	2.208E-11	76.179
^{209}Bi(n,7n)^{203}Bi	55.401	1.079E-14	4.067E-14	1.007	55.153	1.150E-15	2.806E-15	0.013
^{209}Bi(γ,6n)^{203}Bi	72.519	2.051E-13	3.998E-12	98.993	72.560	2.574E-12	2.208E-11	99.987
^{209}Bi(n,8n)^{202}Bi	60.734	2.974E-16	1.120E-15	0.048	60.924	2.872E-17	7.009E-17	0.001
^{209}Bi(γ,7n)^{202}Bi	72.519	1.206E-13	2.352E-12	99.952	72.560	1.389E-12	1.192E-11	99.999
^{209}Bi(n,9n)^{201}Bi	71.141	9.963E-21	3.754E-20	2.6E-05	71.002	5.442E-22	1.328E-21	1.8E-07
^{209}Bi(γ,8n)^{201}Bi	85.127	7.485E-15	1.459E-13	100.000	85.129	8.654E-14	7.425E-13	100.000
^{209}Bi(n,10n)^{200}Bi	87.480	9.663E-25	3.641E-24	1.3E-08	87.952	1.925E-26	4.700E-26	3.4E-11
^{209}Bi(γ,9n)^{200}Bi	94.249	1.385E-15	2.701E-14	100.000	94.249	1.602E-14	1.375E-13	100.000
(n,np+d) and (γ,p) reactions on the same target and leading to production of the same isotope								
^{29}Si(n,d+np)^{28}Al	16.080	9.008E-03	3.394E-02	99.951	15.856	4.226E-03	1.031E-02	99.904
^{29}Si(γ,p)^{28}Al	18.213	8.520E-07	1.661E-05	0.049	18.217	1.154E-06	9.899E-06	0.096
(n,α) and (γ,h) reactions leading to production of the same isotope								
^{27}Al(n,α)^{24}Na	8.668	9.967E-01	3.755E+00	100.000	8.472	6.826E-01	1.666E+00	100.000
^{27}Al(γ,h)^{24}Na	29.928	6.632E-13	1.293E-11	3.4E-10	30.019	1.049E-12	9.003E-12	5.4E-10
^{51}V(n,α)^{48}Sc	9.974	3.778E-02	1.423E-01	100.000	9.737	2.376E-02	5.799E-02	100.000
^{51}V(γ,h)^{48}Sc	36.175	3.254E-14	6.343E-13	4.5E-10	37.207	7.907E-14	6.784E-13	1.2E-09
^{54}Fe(n,α)^{51}Cr	7.429	1.090E+00	4.107E+00	100.000	7.204	8.104E-01	1.978E+00	100.000
^{54}Fe(γ,h)^{51}Cr	36.175	2.386E-12	4.651E-11	1.1E-09	37.207	4.575E-12	3.925E-11	2.0E-09
^{59}Co(n,α)^{56}Mn	8.371	2.166E-01	8.162E-01	100.000	8.127	1.516E-01	3.700E-01	100.000
^{59}Co(γ,h)^{56}Mn	32.780	2.830E-13	5.517E-12	6.8E-10	36.243	4.741E-13	4.067E-12	1.1E-09
^{63}Cu(n,α)^{60}Co	7.272	6.792E-01	2.559E+00	100.000	7.019	5.112E-01	1.248E+00	100.000
^{63}Cu(γ,h)^{60}Co	32.780	9.250E-14	1.803E-12	7.0E-11	36.243	1.929E-13	1.655E-12	1.3E-10

This tendency is valid for competing pairs (γ,f)/(n,f), (γ,xn)/(n,(x+1)n), (γ,p)/(n,np+d) and (γ,h)/(n,α) (the latter pair is out of the axis scales plotted in Figs 4.1 and 4.2). An exception are the inelastic scattering pairs (γ,γ')/(n,n'). We explain this overall tendency as follows: the larger neutron median energy exceeds the gamma energy, the lower should be the neutron induced n-SACS in comparison with γ-SACS since both n- and γ-spectra for the ^{252}Cf(s.f.) and ^{235}U(n_{th},f) radiation sources quickly decrease above the energy of several MeV.

It is worth mentioning that the γ-Fraction value 1% could be considered as a "photonuclear ignorance threshold" or tolerance level. In such cases the contribution from competing photonuclear reactions to the residual production yield could be neglected, since 1% is the highest accuracy presently achievable in the neutron dosimetry measurements.

For the high threshold reactions, when kinematic threshold E_{thr} > 30 MeV or median response energy E50% > 50 MeV, we observe γ-Fraction approaching to 100%. In other words, the total residual production comes to be generated only by photonuclear reaction, whereas the neutron contribution can be neglected. This effect can be explained with the change of the ^{252}Cf(s.f.) and ^{235}U(n_{th},f) gamma energy spectra from exponentially decreasing to the "flat" distribution at the γ-ray energy around 40 MeV, whereas the neutron energy spectra continue to decrease exponentially, see Figs 3.3 - 3.5. Since the high energy part of gamma spectra from these sources are not well established yet, the saturating dependence of the γ-Fraction could vary in future as new information on PFGS will appear.

It should be noted that the competition between the extremely high threshold gamma and neutron reactions could only be estimated on bismuth, since merely the neutron cross sections ^{209}Bi(n,xn) with extreme large multiplicities x = 6 – 10 were evaluated for neutron dosimetry [5] and are presently available. More generally, the similar (n,xn) sets of the high threshold reactions suitable for activation measurements are possible on other mono-isotopic targets such as ^{169}Tm, ^{103}Rh, ^{139}La, ^{175}Lu, ^{197}Au, ^{59}Co, ^{89}Y. However, the scarce experimental data and existing evaluations, which however are non-validated yet, prevent us to perform the assessment of the (γ,xn) and (n,(x+1)n) competition for these targets.

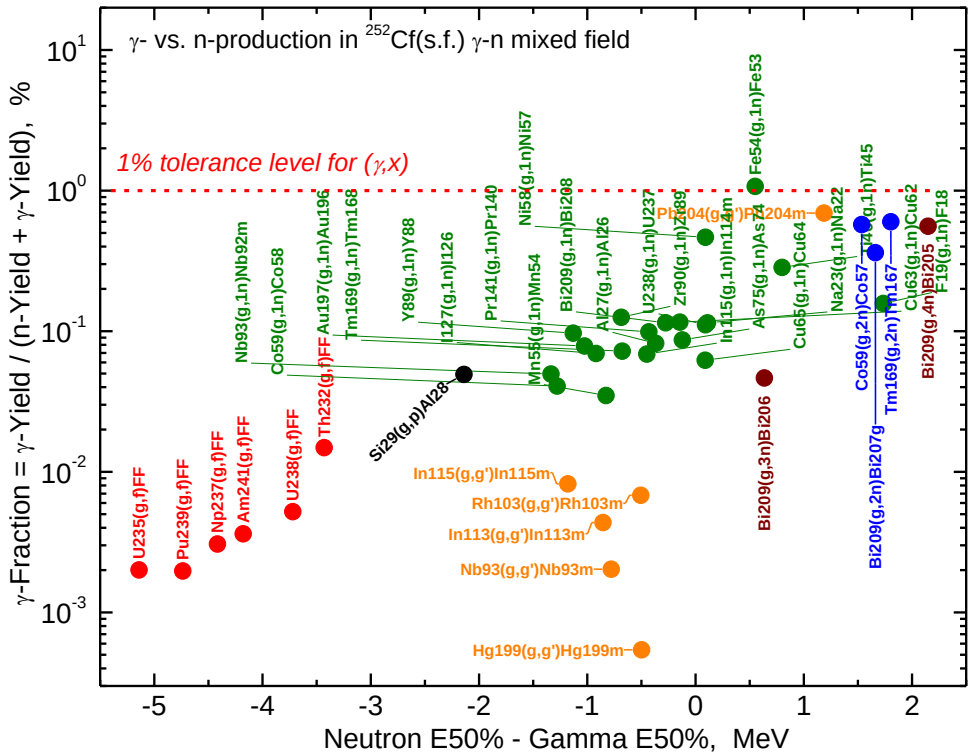

FIG. 4.1 The relative contribution of the (γ,x) reaction to the total (neutron and gamma induced) production of the residuals in the ^{252}Cf(s.f.) mixed n-γ field versus the difference between the neutron and gamma 50% response energies. The following competing reaction pairs are displayed: (γ,f) vs. (n,f), (γ,γ') vs. (n,n'), (γ,(x-1)n) vs. (n,xn) x = 2 - 4, (γ,p) vs. (n,np+d).

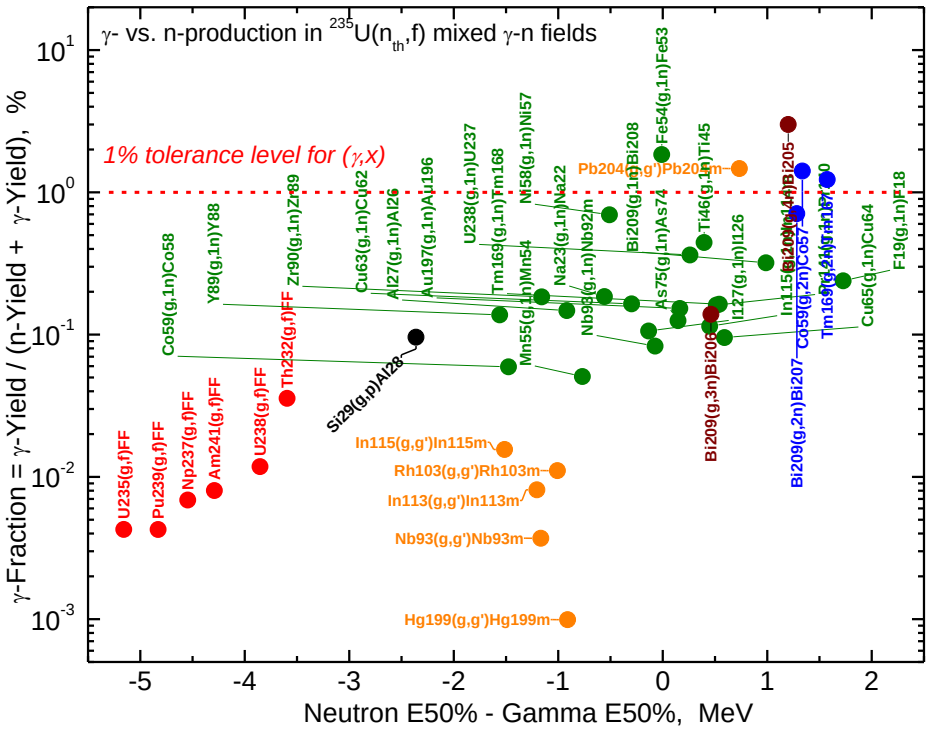

FIG. 4.2. The relative contribution of the (γ,x) reaction to the total (neutron and gamma induced) production of the residuals in the $^{235}U(n_{th},f)$ mixed n-γ field versus the difference between the neutron and gamma 50% response energies. The following competing reaction pairs are plotted: (γ,f) vs. (n,f), (γ,γ') vs. (n,n'), (γ,(x-1)n) vs. (n,xn) x = 2 - 4, (γ,p) vs. (n,np+d).

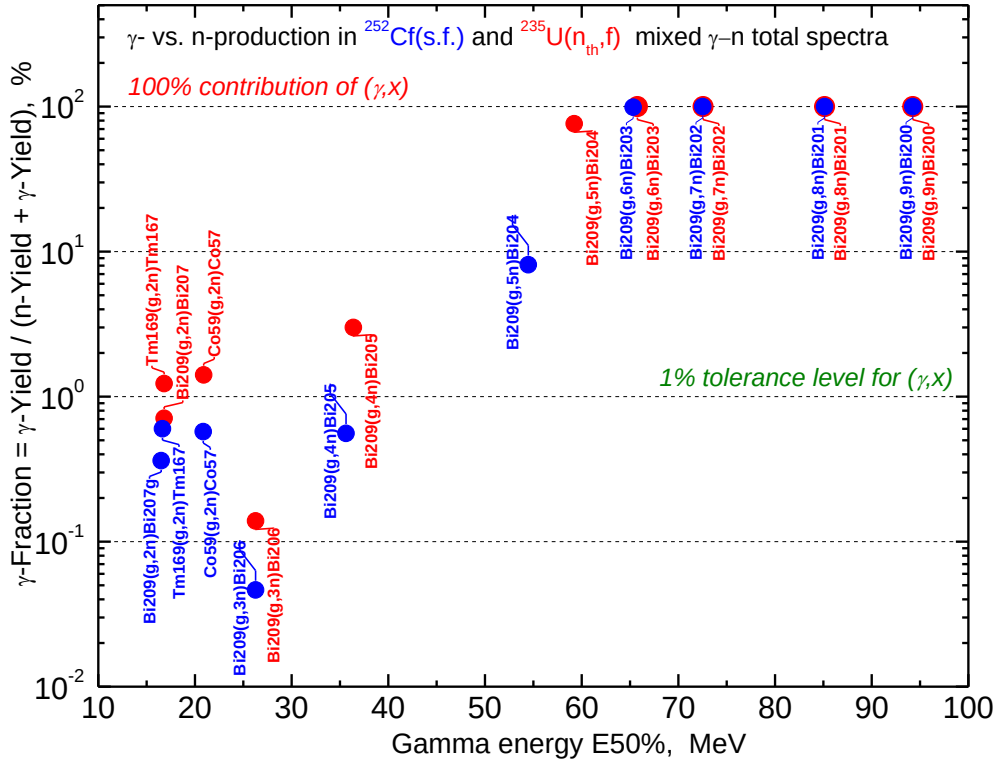

FIG. 4.3. The relative contribution of the (γ,x) reaction to the total (neutron and gamma induced) production of the residuals in the mixed n-γ fields from the $^{252}Cf(s.f.)$ and $^{235}U(n_{th},f)$ sources for the extreme high threshold reactions versus the median response γ-ray energy γ-E50%. The results for competing reaction pairs (γ,xn) and (n,(x+1)n) on ^{59}Co and ^{169}Tm with multiplicity x = 2, and on ^{209}Bi with x = 2 – 9 are displayed.

5. Calculation of the neutron and gamma competition for natural elements

In the previous Section 4 the mono-isotopes as targets for the neutron and gamma induced reactions were considered. In practice, the elemental or not isotopically enriched materials are often used as the neutron dosimeters. In those cases, the photonuclear reactions on some isotopes composing the target element can be additional reaction pathways to the detectable specific residual. Analysing the content of the IRDFF-II library and the isotopic composition of the natural elements, we found 13 neutron dosimetry reactions for which the production of the same final residual by the (γ,x) reactions on other isotopes of the same chemical element is possible.

The list of those competing reactions is summarized in Table 5.1. It includes three types of the neutron dosimetry reactions (n,2n), (n,p) and (n,α) on isotopes which are present in the element with natural abundance less than 100%. For (n,2n) and (n,α), the competing photonuclear reactions (γ,1n) and (γ,h) on the same target isotope are also possible and were already studied in Section 4. They are repeated in Table 5.1 (*in italics*) for comparison of the residual production yields from all possible (γ,x) reactions on all isotopes of the target element. The competition between neutron dosimetry (n,p) and various (γ,x) photonuclear reactions is only conceivable on different target isotopes. The fission reaction pairs (n,f) and (γ,f) were excluded from the present consideration, since the proper dosimeters (ionization chambers, activation foils, etc.) always use the isotopically enriched fissile materials.

The cross sections for the neutron and gamma induced reactions were taken from libraries IRDFF-II [1] and IAEA/PD-2019.2 [3], employing the MF/MT/ZAP combinations listed in Table 5.1. The spectrum averaged cross sections were calculated by code RR_UNC code [34] using the total neutron and gamma absolute fission energy spectra ^{252}Cf(s.f.) or ^{235}U(n_{th},f) described in Section 3.

TABLE 5.1. Possible competing neutron and gamma induced reactions on the elemental targets which lead to the same residual radionuclide.
(*Columns: isotopic Abundancies (Abund) [35], kinematic Thresholds (Thresh) and the file, reaction, product numbers (MF/MT/ZAP) which identify the radionuclide production in the IRDFF-II [1] and IAEA/PD-2019.2 [3] libraries.)*

Neutron induced reactions in IRDFF-II				**Gamma induced reactions in IAEA/PD-2019.2**			
Reaction	Abund, %	Thresh, MeV	Reaction MT/ZAP	Reaction	Abund, %	Thresh, MeV	MF/MT/ ZAP
(n,2n) and (γ,xn) reactions on the different target but leading to production of the same isotope							
^{46}Ti(n,2n)^{45}Ti	8.25	13.479	16	*^{46}Ti(γ,1n)^{45}Ti* [a]	*8.25*	*13.189*	*22045*
				^{47}Ti(γ,2n)^{45}Ti	7.44	22.070	22045
				^{48}Ti(γ,3n)^{45}Ti	73.72	33.697	22045
^{54}Fe(n,2n)^{53}Fe	5.85	13.629	16	*^{54}Fe(γ,1n)^{53}Fe* [a]	*5.85*	*13.378*	*26053*
				^{56}Fe(γ,3n)^{53}Fe	91.75	33.874	26053
^{58}Ni(n,2n)^{57}Ni	68.08	12.429	16	*^{58}Ni(γ,1n)^{57}Ni* [a]	*68.08*	*12.216*	*28057*
				^{60}Ni(γ,3n)^{57}Ni	26.22	*32.603*	28057
^{63}Cu(n,2n)^{62}Cu	30.85	11.038	16	*^{63}Cu(γ,1n)^{62}Cu* [a]	*30.85*	*10.864*	*29062*
				^{65}Cu(γ,3n)^{62}Cu	69.15	28.690	29062
^{90}Zr(n,2n)^{89}Zr	51.45	12.103	16	*^{90}Zr(γ,1n)^{89}Zr* [a]	*51.45*	*11.968*	*10/5/1*
				^{91}Zr(γ,2n)^{89}Zr	11.22	19.162	40089g
				^{92}Zr(γ,3n)^{89}Zr	17.15	27.797	40089g
				^{94}Zr(γ,5n)^{89}Zr	17.38	42.751	40089g
(n,p) and (γ,x) reactions on the different target but leading to production of the same isotope							
^{46}Ti(n,p)^{46}Sc	8.25	1.619	103	^{47}Ti(γ,p)^{46}Sc	7.44	10.465	21046
				^{48}Ti(γ,d)^{46}Sc	73.72	19.867	21046
^{47}Ti(n,p)^{47}Sc	7.44	0.000	103	^{48}Ti(γ,p)^{47}Sc	73.72	11.445	21047
				^{49}Ti(γ,d)^{47}Sc	5.41	17.363	21047
				^{50}Ti(γ,nd)^{47}Sc	5.18	28.302	21047
^{56}Fe(n,p)^{56}Mn	91.75	2.965	103	^{57}Fe(γ,p)^{56}Mn	2.12	10.560	25056
				^{58}Fe(γ,d)^{56}Mn	0.28	18.379	25056
^{67}Zn(n,p)^{67}Cu	4.04	0.000	103	^{68}Zn(γ,p)^{67}Cu	18.45	9.977	29067
^{92}Mo(n,p)^{92m}Nb	14.65	0.000	41092m	^{94}Mo(γ,d)^{92m}Nb	9.19	15.230	41092m
				^{95}Mo(γ,nd)^{92m}Nb	15.87	22.599	41092m
				^{96}Mo(γ,2nd)^{92m}Nb	16.67	31.754	41092m

(n,α) and (γ,x) reactions on the different target but leading to production of the same isotope							
^{51}V(n,α)^{48}Sc	99.75	2.095	107	*^{51}V(γ,h)^{48}Sc* [a]	*0.25*	*22.631*	21048
				^{50}V(γ,d)^{48}Sc	0.25	17.856	21048
^{54}Fe(n,α)^{51}Cr	5.85	0.000	107	*^{54}Fe(γ,h)^{51}Cr* [a]	*5.85*	*19.734*	24051
				^{56}Fe(γ,nα)^{51}Cr	91.75	19.652	24051
^{63}Cu(n,α)^{60}Co	69.15	0.000	107	*^{65}Cu(γ,h)^{60}Co* [a]	*69.15*	*20.249*	27060
				^{65}Cu(γ,nα)^{60}Co	30.85	16.110	27060

Note: a) the (γ,x) and (n,y) competing reactions on the same target isotope (already considered in Section 4).

The relative neutron and gamma contributions to the residual production, relative n- and γ-Fractions, on the natural target from the specific isotope *i* of the target element were calculated following the equations:

$$n-Fraction_i = \frac{n-Yield_i}{\sum_i \gamma-Yield_i + n-Yield_i} = \frac{Abund_i \times n-SACS_i \times Mn}{\sum_i (Abund_i \times \gamma-SACS_i) \times M\gamma + n-SACS_i \times Mn} \quad (5.1)$$

$$\gamma-Fraction_i = \frac{\gamma-Yield_i}{\sum_i \gamma-Yield_i + n-Yield_i} = \frac{Abund_i \times \gamma-SACS_i \times M\gamma}{\sum_i (Abund_i \times \gamma-SACS_i) \times M\gamma + n-SACS_i \times Mn} \quad (5.2),$$

where:

- γ-Yield$_i$ = Abund$_i$ × γ-SACS$_i$ × Mγ – gamma induced reaction Yield on isotope *i* of element,
- n-Yield$_i$ = Abund$_i$ × n-SACS$_i$ × Mn – neutron induced reaction Yield on isotope *i* of element,
- Abund$_i$ – abundance of isotope *i* in natural element which is a target for neutrons or gammas,
- Mγ and Mn – total gamma and neutron Multiplicities per fission event of ^{252}Cf(s.f.) or ^{235}U(n$_{th}$,f).

The calculation results are listed in Table 5.2. It can be seen that the gamma induced production on all other target isotopes of the target natural element, is smaller than ≈ 10^{-4}% relative to the neutron induced production. These "cross-isotope" γ-Fractions are even smaller than one on the same target isotope. Such a combination occurs with the (n,2n) and (n,α) neutron dosimetry reactions, but not for (n,p).

TABLE 5.2. The γ-ray induced reactions competing with the IRDFF-II neutron dosimetry reactions on natural targets in ^{252}Cf(s.f.) and ^{235}U(n$_{th}$,f) mixed n-γ radiation fields:
(Columns: 50% response energy (E50%), spectrum averaged cross section (SACS), residual production yield (Yield) per fission event, and relative contribution (Fraction) to the total residual production. The photonuclear reactions are highlighted by red font for simplicity of comparison with neutron dosimetry ones.)

Competing Reactions	^{252}Cf(s.f.) mixed n- and γ-fields				^{235}U(n$_{th}$,f) mixed n- and γ-fields			
	E50%, MeV	SACS, mb	Yield, mb/f	Fraction,%	E50%, MeV	SACS, mb	Yield, mb	Fraction,%
(n,2n) and (γ,xn) reactions leading to the same residual								
^{46}Ti(n,2n)^{45}Ti	16.107	1.225E-02	2.466E-03	9.98E+01	16.005	5.648E-03	1.137E-03	9.96E+01
^{46}Ti(γ,1n)^{45}Ti	*15.306*	*6.750E-06*	4.777E-06	*1.93E-01*	*15.609*	*7.170E-06*	5.075E-06	*4.44E-01*
^{47}Ti(γ,2n)^{45}Ti	24.664	1.531E-09	9.773E-10	3.96E-05	24.664	2.347E-09	1.498E-09	1.31E-04
^{48}Ti(γ,3n)^{45}Ti	39.700	1.110E-13	7.022E-13	2.84E-08	44.771	3.123E-13	1.975E-12	1.73E-07
^{54}Fe(n,2n)^{53}Fe	16.592	3.559E-03	5.082E-04	9.93E+01	16.494	1.614E-03	2.304E-04	9.82E+01
^{54}Fe(γ,1n)^{53}Fe	*16.042*	*7.451E-06*	*3.740E-06*	*7.30E-01*	*16.504*	*8.631E-06*	*4.332E-06*	*1.85E+00*
^{56}Fe(γ,3n)^{53}Fe	40.662	4.676E-14	3.681E-13	7.19E-08	49.416	1.549E-13	1.219E-12	5.19E-07
^{58}Ni(n,2n)^{57}Ni	14.980	8.441E-03	1.403E-02	9.97E+01	14.879	4.077E-03	6.775E-03	9.93E+01
^{58}Ni(γ,1n)^{57}Ni	*14.889*	*7.634E-06*	*4.459E-05*	*3.17E-01*	*15.389*	*8.126E-06*	*4.746E-05*	*6.96E-01*
^{60}Ni(γ,3n)^{57}Ni	37.123	1.232E-13	2.770E-13	1.97E-09	38.233	2.519E-13	5.665E-13	8.30E-09
^{63}Cu(n,2n)^{62}Cu	13.838	1.945E-01	1.464E-01	9.99E+01	13.721	9.898E-02	7.453E-02	9.98E+01
^{63}Cu(γ1,n)^{62}Cu	*13.983*	*4.364E-05*	*1.155E-04*	*7.88E-02*	*14.019*	*4.640E-05*	*1.228E-04*	*1.64E-01*
^{65}Cu(γ,3n)^{62}Cu	33.138	9.329E-12	5.534E-11	3.78E-08	33.186	1.454E-11	8.627E-11	1.16E-07
^{90}Zr(n,2n)^{89}Zr	14.420	2.131E-01	2.676E-01	9.99E+01	14.320	1.054E-01	1.323E-01	9.98E+01
^{90}Zr(γ,1n)^{89}Zr	*15.106*	*5.177E-05*	2.285E-04	*8.53E-02*	*15.478*	*5.532E-05*	2.442E-04	*1.84E-01*
^{91}Zr(γ,2n)^{89}Zr	20.165	1.081E-07	1.040E-07	3.88E-05	20.245	1.540E-07	1.482E-07	1.12E-04
^{92}Zr(γ,3n)^{89}Zr	31.992	1.786E-11	2.628E-11	9.81E-09	32.087	2.823E-11	4.154E-11	3.13E-08
^{94}Zr(γ,5n)^{89}Zr	66.427	9.018E-14	1.345E-13	5.02E-11	67.438	9.763E-13	1.456E-12	1.10E-09

(n,p) and (γ,x) reactions leading to the same residual								
^{46}Ti(n,p)^{46}Sc	6.079	1.356E+01	2.730E+00	1.00E+02	5.862	1.104E+01	2.224E+00	1.00E+02
^{47}Ti(γ,p)^{46}Sc	16.337	1.055E-06	6.735E-07	2.47E-05	16.776	1.263E-06	8.060E-07	3.62E-05
^{48}Ti(γ,d)^{46}Sc	27.291	4.157E-11	2.629E-10	9.63E-09	27.304	6.398E-11	4.046E-10	1.82E-08
^{47}Ti(n,p)^{47}Sc	3.810	1.924E+01	3.493E+00	1.00E+02	3.647	1.765E+01	3.205E+00	1.00E+02
^{48}Ti(γ,p)^{47}Sc	16.793	3.060E-07	1.936E-06	5.54E-05	17.022	3.882E-07	2.455E-06	7.66E-05
^{49}Ti(γ,d)^{47}Sc	23.978	1.054E-09	4.890E-10	1.40E-08	23.981	1.613E-09	7.487E-10	2.34E-08
^{50}Ti(γ,nd)^{47}Sc	36.324	3.888E-13	1.728E-13	4.95E-12	44.700	1.061E-12	4.715E-13	1.47E-11
^{56}Fe(n,p)^{56}Mn	7.578	1.434E+00	3.212E+00	1.00E+02	7.362	1.051E+00	2.354E+00	1.00E+02
^{57}Fe(γ,p)^{56}Mn	16.231	1.085E-06	1.974E-07	6.14E-06	16.575	1.289E-06	2.344E-07	9.96E-06
^{58}Fe(γ,p)^{56}Mn	25.743	2.229E-10	5.354E-12	1.67E-10	25.746	3.420E-10	8.215E-12	3.49E-10
^{67}Zn(n,p)^{67}Cu	4.702	1.087E+00	1.072E-01	1.00E+02	4.421	9.472E-01	9.340E-02	1.00E+02
^{58}Zn(γ,n)^{57}Ni	14.956	4.049E-07	6.409E-07	5.98E-04	15.245	4.231E-07	6.697E-07	7.17E-04
^{92}Mo(n,p)^{92m}Nb	5.388	7.684E+00	2.748E+00	1.00E+02	5.190	6.529E+00	2.335E+00	1.00E+02
^{94}Mo(g,d)^{92m}Nb	23.310	9.978E-10	7.867E-10	2.86E-08	23.316	1.527E-09	1.204E-09	5.16E-08
^{95}Mo(g,nd)^{92m}Nb	27.472	8.154E-12	1.110E-11	4.04E-10	27.793	1.287E-11	1.752E-11	7.50E-10
^{96}Mo(n,2nd)^{92m}Nb	42.880	8.471E-14	1.211E-13	4.41E-12	65.312	4.689E-13	6.706E-13	2.87E-11
(n,α) and (γ,x) reactions leading to production of the same isotope								
^{51}V(n,α)^{48}Sc	9.974	3.778E-02	9.199E-02	1.00E+02	9.737	2.376E-02	5.784E-02	1.00E+02
^{51}V(γ,h)^{48}Sc	*33.949*	*3.254E-14*	*2.784E-13*	*3.03E-10*	*39.654*	*7.907E-14*	*6.767E-13*	*1.17E-09*
^{51}V(γ,d)^{48}Sc	26.620	6.967E-12	1.494E-13	1.62E-10	26.624	1.069E-11	2.293E-13	3.96E-10
^{54}Fe(n,α)^{51}Cr	7.429	1.090E+00	1.557E-01	1.00E+02	7.204	8.104E-01	1.157E-01	1.00E+02
^{54}Fe(γ,h)^{51}Cr	*36.175*	*2.386E-12*	*1.197E-12*	*7.69E-10*	*37.207*	*4.575E-12*	*2.296E-12*	*1.98E-09*
^{56}Fe(γ,na)^{51}Cr	28.985	6.713E-12	5.284E-11	3.39E-08	29.089	1.064E-11	8.373E-11	7.24E-08
^{63}Cu(n,α)^{60}Co	7.272	6.792E-01	1.146E+00	1.00E+02	7.019	5.112E-01	8.627E-01	1.00E+02
^{63}Cu(γ,h)^{60}Co	*32.780*	*9.250E-14*	*5.487E-13*	*4.79E-11*	*36.243*	*1.929E-13*	*1.145E-12*	*1.33E-10*
^{65}Cu(γ,na)^{60}Co	25.957	2.292E-11	6.066E-11	5.29E-09	36.243	1.929E-13	5.106E-13	5.92E-11

6. Options to validate the extreme high energy part of ^{252}Cf(s.f.) and ^{235}U(nth,f) PFGS

In Section 4 it was stated that γ-Yield and γ-Fraction for extremely high threshold reactions substantially depend on the absolute value and energy shape of the ^{252}Cf(s.f.) and ^{235}U(n_{th},f) prompt fission gamma spectra, which are questionable for Eγ > 40 MeV. It may be of interest to use those reactions for the experimental determination of this energy part of PFGS. Table 6.1 lists a set of reactions (γ,xn) and (n,(x+1)n), where multiplicity x = 1 – 9, on monoisotopic element ^{209}Bi that produce unstable radionuclides $^{209-x}$Bi. For the first group of reactions (when x ≤ 4), the kinematic threshold Ethr < 30 MeV (see Table 2.1) or median response energy E50% < 38 MeV (Table 4.1). For them, the contribution of (γ,xn) to the total residual production or γ-Fraction < 3% (Table 4.1), i.e. the neutron induced production dominates. For the second group of reactions (x ≥ 5) the situation is vice versa, i.e. the total residual yield results from the gamma induced reactions.

Table 6.1 lists the absolute total (sum of gamma and neutron induced) yields of residuals and their half-lives. The decay of residual radionuclides (all goes via the electron capture EC or positron emission β^+ modes with 100% probability) creates the daughter isotopes. The important radiation characteristics used in the activation measurements are also listed in this table: the energy of the most dominant γ-rays and absolute emission intensity per residual radionuclide decay event. The γ-ray emission rate *γ-Rate* at zero cooling time (*t = 0)* was then calculated per one ^{252}Cf(s.f.) or ^{235}U(n_{th},f) fission event:

$$\gamma - Rate = \exp\left(-(t=0) \times \ln(2)/T_{1/2}\,(Res)\right) \times \ln(2)/\,T_{1/2}\,(Res) \qquad (6.1)$$

where:

- $T_{1/2}(Res)$ – half-life of the reaction residual radionuclide,
- I_γ – γ-ray emission per one decay of the reaction residual.

TABLE 6.1. Reactions ^{209}Bi(γ,xn) and ^{209}Bi(n,(x+1)n), x = 1 – 9, that produce the same residuals (Res) $^{209-x}$Bi, the total (neutron + gamma) residual yield (Yield) and residual have half-lives $T_{1/2}$(Res).
(Decay of the residuals: their daughter isotopes (Iso), the most prominent decay γ-ray energies (E_γ) and intensities (I_γ), absolute emission gamma rate (γ-Rate) and relative rate (Rel. γ-Rate) normalized to ^{206}Pb (highlighted by bold font). The last column contains further decay chains of daughter isotopes to the quasi-stable (half life > 50 000 y) or stable isotopes, in bold.)

Contributing γ- and n-Reactions	Reaction Residual			Daughter of Residual Decay					Daughter' further decay chain
	Res[a]	Yield, mb/f	$T_{1/2}$(Res)	Iso	E_γ, keV	I_γ, %	γ-Rate mb/f/s	Rel. γ-Rate	
^{209}Bi(γ,xn) and ^{209}Bi(n,(x+1)n), x = 1 – 4, having the kinematic threshold < 30 MeV or E50% < 38 MeV									
^{209}Bi(γ,1n)+(n,2n)	^{208}Bi	3.7E+01	3.7 10^{+5} y	**^{208}Pb**	2614.5	99.8	2.2E-12	0.021	stable
^{209}Bi(γ,2n)+(n,3n)	^{207}Bi	6.9E-02	31.63 y	**^{207}Pb**	569.7	97.8	4.7E-11	0.437	stable
^{209}Bi(γ,3n)+(n,4n)	^{206}Bi	8.4E-05	6.24 d	**^{206}Pb**	803.1	99.0	**1.1E-10**	**1.000**	stable
^{209}Bi(γ,4n)+(n,5n)	^{205}Bi	4.8E-08	14.91 d	**^{205}Pb**	1764.3	32.4	8.4E-14	7.9E-05	$\xrightarrow{1.7\,E+7\,y}$ **^{205}Tl**
^{209}Bi(γ,xn) and ^{209}Bi(n,(x+1)n), x = 5 – 10, having the kinematic threshold > 38 MeV or E50% > 46 MeV									
^{209}Bi(γ,5n)+(n,6n)	^{204}Bi	7.5E-11	11.22 h	**^{204}Pb**	899.2	99.0	1.3E-15	1.2E-05	stable
^{209}Bi(γ,6n)+(n,7n)	^{203}Bi	4.0E-12	11.76 h	^{203}Pb	820.2	29.7	2.0E-17	1.8E-07	$\xrightarrow{2.2\,d}$ **^{203}Tl**
^{209}Bi(γ,7n)+(n,8n)	^{202}Bi	2.4E-12	1.71 h	**^{202}Pb**	960.7	99.3	2.6E-16	2.5E-06	$\xrightarrow{52\,ky}$ ^{202}Tl $\xrightarrow{12\,d}$ **^{202}Hg**
^{209}Bi(γ,8n)+(n,9n)	^{201}Bi	1.5E-13	1.72 h	^{201}Pb	629.1	24.7	4.0E-18	3.8E-08	$\xrightarrow{9.3\,h}$ ^{201}Tl $\xrightarrow{3.0\,d}$ **^{201}Hg**
^{209}Bi(γ,9n)+(n,10n)	^{200}Bi	2.7E-14	0.61 h	^{200}Pb	1026.5	99.0	8.5E-18	8.0E-08	$\xrightarrow{22\,h}$ ^{200}Tl $\xrightarrow{26\,h}$ **^{200}Hg**

Note: a) all the ^{209}Bi(γ,xn) or ^{209}Bi(n,(x+1)n) reaction residuals $^{209-x}$Bi are unstable and decay via EC or β^+ modes.

The *relative γ-Rate* was calculated after normalization per maximal rate, i.e. per *γ-Rate* for emission of 803.1 keV from decay of ^{206}Bi. This is the most intensive discrete γ-ray emission yield in the first group of reactions ^{209}Bi(γ,xn) and ^{209}Bi(n,(x+1)n) with multiplicity lower than 4, which could be used as a reference or scale.

For the second group of reactions ^{209}Bi(γ,xn + n,(x+1)n), $x \geq 5$, the total reaction residual yields or relative gamma rates substantially depend on the value of the high energy part of PFGS. Since the relative γ-ray rate for these reactions is small and decreases from around 1 10^{-5} to 4 10^{-8} as neutron multiplicity *x* increases (see Table 6.1), the feasibility of activation measurements becomes questionable. To get a preliminary answer we searched the high threshold ^{209}Bi(γ,xn) and ^{209}Bi(n,(x+1)n) activation measurements carried out with the fission or continues neutron and gamma spectra in the literature and EXFOR database [7].

n-SACS measured in the ^{252}Cf(s.f.) and ^{235}U(n_{th},f) fields. M. Schulc et al. [36] measured n-SACS for reactions ^{209}Bi(n,xn) with the highest neutron multiplicity x = 3 and 4 using the activation technique and employing the ^{252}Cf(s.f.) source. They detected 569.7 keV and 1.063.7 keV γ-ray activities from decay of ^{207}Bi and 803.1 keV and 122.1 keV γ-rays from ^{206}Bi. This team also used the same method to measure the n-SACS for reactions ^{209}Bi(n,3n)^{207}Bi and ^{209}Bi(n,4n)^{206}Bi in the ^{235}U(n_{th},f) prompt fission neutron spectrum which was generated at the research reactor LVR-15 [37]. n-SACS for ^{209}Bi(n,3n)^{207}Bi was also measured using the activation technique in the ^{239}Pu(n,f) prompt fission neutron spectrum at the IBR-2 reactor loaded with plutonium dioxide fuel [38].

The authors of the experiments carried out in [36], [38] obviously supposed as default that the impact of gamma induced reactions is negligible. The results obtained in the present work confirm this quantitively: the impact of photonuclear reactions on residual production, γ-Fraction, amounts only ≈ 0.05% or 0.14% for pair ^{209}Bi(γ,3n)^{206}Bi and ^{209}Bi(n,4n)^{206}Bi in the ^{252}Cf(s.f.) or ^{235}U(n_{th},f) n-γ mixed fields, respectively (see Table 4.1).

n-Rates measured in the accelerator driven source (ADS) fields. J. Adam et al. measured residual decay rates for reactions ^{209}Bi(n,xn) where neutron multiplicity *x* varied between 4 and 9 [39], [40]. The source of neutrons was a 20 cm long lead target surrounded by a 6 cm paraffin moderator and irradiated by a 1 GeV proton beam.

The bismuth samples of 2.5 mm thickness were placed at the end of lead target. Authors calculated the neutron spectrum at the Bi sample position with the help of the intranuclear cascade and transport code CASCADE up to neutron energy ≈ 600 MeV. They wrote: " *... the calculated reaction rates below a threshold energy of 30 MeV are 10 - 30% lower than the experimental reaction rates, but the reaction rates become much lower (up to factor 2) at higher neutron energies. Such a trend was observed for all samples. Although there is a deviation from this trend for Co*" [39].

It should be noted that the gamma spectrum at the bismuth sample position was not considered by the authors of experiment [39], [40]. Hence, the ignorance of photonuclear reactions in the analysis of this experiment could be a reason of the systematic underestimations for such extreme high threshold neutron reactions as ^{209}Bi(n,xn) with multiplicity $x = 4 – 9$ that was observed in this experiment.

γ-Yield or γ-SACS measured in the bremsstrahlung radiation produced by electron beams. A. Ermakov, S. Belyshev and co-workers measured the yields of $^{209-x}$Bi produced by photonuclear reactions ^{209}Bi(γ,xn) with neutron multiplicity $x = 2 – 7$ [41] and $x = 2 – 6$ [42] using the activation technique. The bismuth samples were exposed to the bremsstrahlung photons produced by an electron beam striking a tungsten convertor. The electrons were accelerated by microtrons up to energy 67.7 or 55.6 MeV. The authors observed good agreement between the experimental and theoretical yields of radionuclides generated by photo-neutron reactions on the ^{209}Bi nucleus. The theoretical yields were obtained by folding of the photonuclear cross sections calculated by reaction models and bremsstrahlung spectrum simulated by code GEANT4.

Similar measurements were performed by H. Naik et al. at the electron linear accelerator which was operated at energies in between 50 and 70 MeV [43]. The bremsstrahlung photons were produced in the tungsten target. The gamma induced spectrum average cross sections for reactions ^{209}Bi(γ,xn) with multiplicities $x = 2 – 6$ were measured. They were also theoretically calculated by the nuclear model code TALYS 1.0. The distribution of the photon flux for bremsstrahlung at different electron energies was calculated by GEANT4. The authors found that the flux-weighted average theoretical cross-sections for ^{209}Bi(γ,(3-6)n) are in good agreement with the experimental values.

We would like to point out the following. The bremsstrahlung gamma spectrum produced by a beam of electrons in heavy targets has maximum at ≈ 1 MeV and decreases by 3 – 4 orders of magnitude until the γ-ray end-point energy which is equal to the energy of electrons, e.g. see [43]. These high energy gammas may produce secondary neutrons in the target via photo-neutron reactions. Probably this two-step mechanism results in the very small fraction of neutrons in comparison with the bremsstrahlung gammas. Consequently, the contribution of neutron induced reactions to the residual production is indeed negligible in comparison with the photonuclear pathway.

Summary on feasibility of the high energy threshold ^{209}Bi(γ,xn) and ^{209}Bi(n,(x+1)n) measurements in the ^{252}Cf(s.f.) and ^{235}U(n_{th},f) fields.

The neutron and gamma induced spectrum averaged cross sections, yields or decay radiation rates for the highest neutron multiplicities up to 7 – 9 were measured for bismuth at the accelerator driven sources. The radiation fields are dominated by either neutrons (charged ion induced spallation) or gammas (electron induced bremsstrahlung). Moreover, these facility energy spectra fall towards the higher energy more slowly than the neutron and gamma spectra in the case of ^{252}Cf(s.f.) and ^{235}U(n_{th},f). All known measurements at the accelerate driven sources were carried out using the activation technique.

For the reactions on bismuth in the ^{252}Cf(s.f.) and ^{235}U(n_{th},f) mixed radiation fields the maximum neutron multiplicity achieved so far is only 4. The known measurements were carried out in one single lab using the activation technique. Since the residual yield or γ-decay rate decreases further by an order of magnitude per every additional neutron multiplicity, it will probably be difficult to measure the extreme high threshold photonuclear reactions which are sensitive to the shape of PFGS above ≈ 45 MeV. An alternative could be the mass spectrometry analysis, e.g. see [44], with which the yield of (quasi) stable isotopes eventually produced in decay chains of residuals could be measured.

7. Summary

For the first time, the systematic competition between the neutron and gamma induced reactions leading to the same residuals in the ^{252}Cf(s.f.) and ^{235}U(n_{th},f) neutron-gamma mixed radiation fields was studied. The neutron reactions selected for this study were those included in IRFFF-II – a reference library recommended for neutron dosimetry. The competing photonuclear cross sections were taken primarily from the IAEA/PD-2019, a reference photo-nuclear library, or from TENDL-2023, a general-purpose cross section library.

The contribution of the competing reactions to the total residual production was numerically estimated employing the Spectrum Averaged Cross Sections (SACS) calculated in the neutron and gamma spectra. For the ^{252}Cf(s.f.) and ^{235}U(n_{th},f) radiations the prompt and delayed fission neutron and gamma spectra (PFNS and DFNS, PFGS and DFGS) were considered. They were taken from the Neutron Standards or ENDF/B-VIII.0 evaluations up to radiation energies 20 - 30 MeV. For estimation of radionuclide production competition between the high threshold reactions, the radiation spectra were extrapolated up to 100 - 200 MeV following the energy trend (in case of PFNS) or using the measured upper limits (for PFGS).

For the mono isotopic targets, 39 neutron induced reactions were found in IRDFF-II, for which the (γ,x) path-ways also exist and lead to the production of the same residuals. These reaction pairs turned out to be: (n,f) and (γ,f), (n,n') and (γ,γ'), (n,xn) and (γ,(x-1)n) where x = 2 - 5, (n,np+d) and (γ,p), (n,α) and (n,h). It was shown that the impact of (γ,x) on production, or the relative γ-Fraction, varies from around 10^{-10}% to 100%. For most of the reactions considered, the γ-ray impact was shown to be lower than 1% and thus could be neglected, since this value is comparable with the highest accuracy achievable in the actual neutron dosimetry measurements. The maximum γ-Fraction, 1 - 2%, was observed for the competing reactions ^{54}Fe(γ,n)^{53}Fe and ^{54}Fe(n,2n)^{53}Fe.

For the high threshold reactions ^{209}Bi(n,xn) x = 6 – 10 with kinematic threshold above 30 MeV, the γ-Fraction reaches 100%. This trend reflects the change of the ^{252}Cf(s.f.) and ^{235}U(n_{th},f) gamma energy spectra from exponentially decreasing to the "flat" distribution at the γ-ray energy around 40 MeV, whereas the neutron energy spectra were supposed to continue exponential falling. Since the high energy part of gamma spectra from these sources are not well established yet, the saturating dependence of the γ-Fraction could change in the future. The decreasing yield of residuals by one order of magnitude per every multiplicity makes the activation experiment not easy to realize. As an alternative, the accelerator mass spectrometry could be considered for experimental proof of the PFGS high energy tail.

In addition to the mono-isotope targets, the elemental targets were also considered. For them the (γ,x) reactions on other isotopes of element could also make a contribution to the production of residuals. 13 such elemental targets were found in the IRDFF-II library. The estimation of the photonuclear impact on residual production was found to be below than 10^{-4} percent, which is insignificant in comparison with the neutron pathways to residual.

The studies performed in the present work concentrated on competition between the gamma and neutron induced reactions in the ideal ^{252}Cf(s.f.) and ^{235}U(n_{th},f) γ-n mixed fields (i.e. without perturbation from any surrounding materials). Within this context, we would like to refer to the recent experimental and simulation studies at the research reactors VR-1 and LR-0 [45], [46]. There it was shown that engineering structures present in the reactor core could be a source of additional gammas which explain ≈ (10 - 20)% of reaction residuals produced by neutrons [45].

Acknowledgment

The author of this report should like to thank R. Capote from the IAEA Nuclear Data Section for his interest and discussions stimulating this work.

References

[1] A. Trkov, P.J. Griffin, S.P. Simakov, et al., IRDFF-II: A New Neutron Metrology Library, Nuclear Data Sheets 163 (2020) 1; IRDF-II web-page: https://www-nds.iaea.org/IRDFF/.

[2] S. Simakov, Manage and technical contribution of NDS to CRP on the IRDFF testing, improving and validation, in: Report INDC(NDS)-0731, p. 19, Vienna 2017.

[3] T. Kawano, Y.S. Cho, P. Dimitriou, et al., IAEA Photonuclear Data Library 2019, Nuclear Data Sheets 163 (2020) 109; IAEA/PD-2019 web-page: https://www-nds.iaea.org/photonuclear/.

[4] A.J. Koning, D. Rochman, J. Sublet et al., TENDL: Complete Nuclear Data Library for Innovative Nuclear Science and Technology, Nuclear Data Sheets 155 (2019) 1; TENDL-2023 Gamma sub-library.

[5] V. Pronyaev, preliminary evaluation for ^{209}Bi(n,xn), x = 3-10, E < 100 MeV, on web page https://www-nds.iaea.org/IRDFFtest/.

[6] W.J. Huang, M. Wang, et al., The AME 2020 atomic mass evaluation (I). Evaluation of input data, and adjustment procedures, Chinese Phys. C45 (2021) 030002 and M. Wang, W.J. Huang, et al., The AME 2020 atomic mass evaluation (II). Tables, graphs and references, Chinese Phys. C45 (2021) 030003; AME 2020 web-page: https://www-nds.iaea.org/amdc/.

[7] N. Otuka, E. Dupont, V. Semkova et al., Towards a More Complete and Accurate Experimental Nuclear Reaction Data Library (EXFOR): International collaboration between Nuclear Reaction Data Centres (NRDC), Nuclear Data Sheets 120 (2014) 272.

[8] M.S. Uddin, S. Kamada, et al., Measurements of neutron induced activation of concrete at 64.5 MeV, Ann. Nucl. Energy 38 (2009) 1133.

[9] E. Kim, T. Nakamura, et al., Measurements of neutron spallation cross sections of ^{12}C and ^{209}Bi in the 20- to 150-MeV energy range, Nucl. Sci. and Eng. 129 (1998) 209 .

[10] J. Vrzalová, A. Krása, et al,, Excitation functions of neutron-induced threshold reactions in Au, Bi, Ta measured using 30–94 MeV quasi mono-energetic neutron sources, Nucl. Phys. A1031 (2023) 122593.

[11] NEA Nuclear data high priority request list: HPRL (dosimetry cross section request identification ID 93).

[12] H. Kawada, J.-C. Sublet, S. Okumura, T. Kawano, Processing of the Evaluated Photonuclear Data Library (IAEA/PD-2019), IAEA-NDS-0232, Vienna 2020.

[13] D.E. Cullen, PREPRO 2023 - ENDF/B Pre-processing Codes, Report IAEA-NDS-0241, June 2023, IAEA, Vienna; web-page: PREPRO 2023.

[14] W. Mannhart, Status of the ^{252}Cf fission-neutron evaluation with regard to recent experiments, in: Proc. Consult. Meeting on Physics of Neutron Emission in Fission (24-27 May 1988, Mito Japan), H.D. Lemmel (Ed.), Report INDC(NDS)-220, IAEA, Vienna 1989, p. 305.

[15] A.D. Carlson, V.G. Pronyaev, R. Capote, et al., Evaluation of the Neutron Data Standards, Nuclear Data Sheets 148 (2018) 143.

[16] IAEA NEUTRON DATA STANDARDS: https://www-nds.iaea.org/standards/.

[17] D.A. Brown, M.B. Chadwick, R. Capote, et al., ENDF/B-VIII.0: The 8th Major Release of the Nuclear Reaction Data Library with CIELO-project Cross Sections, New Standards and Thermal Scattering Data, Nuclear Data Sheets 148 (2018) 1.

[18] NEA/OECD Nuclear Data Services: https://www.oecd-nea.org/dbdata/ .

[19] E.J. Axton, Evaluation of the thermal constants of ^{233}U, ^{235}U, ^{239}Pu and ^{241}Pu, and the fission neutron yield of ^{252}Cf, Report GE/PH/01/86, Central Bureau for Nuclear Measurements, Geel, 1986.

[20] T.R. England, ENDF/B-VIII.0 file for ^{252}Cf(s.f.) data, MAT 3644, private communication (1990).

[21] S. Simakov, Evaluation of the prompt gamma-ray spectrum from spontaneous fission of ^{252}Cf, Report INDC(NDS)-0887, Feb 2024, IAEA.

[22] D.H. Stoddard, Radiation Properties of Californium-252, Report DP-986, 1965, Savannah River Lab, Aiken, SC, USA.

[23] D.H. Stoddard and H.E. Hootman, ^{252}Cf Shielding guide, Report DP-1246, 1971, Savannah River Lab, Aiken, SC, USA.

[24] A. Trkov, R. Capote, V.G. Pronyaev, Current Issues in Nuclear Data Evaluation Methodology: U-235 Prompt Fission Neutron Spectra and Multiplicity for Thermal Neutrons, Nucl. Data Sheets **123** (2015) 8.

[25] A. Trkov, R. Capote, Evaluation of the Prompt Fission Neutron Spectrum of Thermal-neutron Induced Fission in U-235, Phys. Proc. **64** (2015) 48.

[26] I. Stetcu, P. Talou, T. Kawano and M. Jandel, Properties of prompt-fission γ rays, Phys. Rev. C90 (2014) 024617.
[27] A. Oberstedt, T. Belgya, R. Billnert, et al., Improved values for the characteristics of prompt-fission γ-ray spectra from the reaction $^{235}U(n_{th},f)$, Phys. Rev. C87 (2013) 051602.
[28] I. Stetcu, M.B. Chadwick, T. Kawano, et al., Evaluation of the Prompt Fission Gamma Properties for Neutron Induced Fission of $^{235,238}U$ and ^{239}Pu (sciencedirectassets.com), Nuclear Data Sheets 163 (2020) 261.
[29] D. Pandit, S. Mukhopadhyay, S. Bhattacharya, et al., Coherent bremsstrahlung and GDR width from ^{252}Cf cold fission, Physics Letters B**690** (2010) 473.
[30] V.A. Varlachev, G.N. Dudkin, V.N. Padalko, Study of the high-energy part spectrum of gamma-rays from the neutron-induced fission reaction, Bull. Russian Academy of Sciences - Physics 71 (2007) 1635.
[31] V.A. Varlachev, G.N. Dudkin, V.N. Padalko, Does the Coherent Bremsstrahlung of Fission Fragments Exist ?, Zhurnal Eksper. i Teoret. Fiz., Pisma v Redakt 82 (2005) 440.
[32] H. Makii, K. Nishio, K. Hirose, et al., Effects of the nuclear structure of fission fragments on the high-energy prompt fission gamma-ray spectrum in $^{235}U(n_{th},f)$, Phys Rev C100 (2019) 044610.
[33] T. Wright, A.G. Smith, N.V. Sosnin et al., Measurement of the prompt fission γ -rays from slow neutron-induced fission of ^{235}U with STEFF, Eur. Phys. J. A60 (2024) 70.
[34] A. Trkov, Program RR_UNC - calculates uncertainties in reaction rates and cross sections; code is available on IRDFF-II web-page: https://www-nds.iaea.org/IRDFF/.
[35] Isotopic Composition of Elements from the Commission on Isotopic Abundances and Atomic Weights (CIAAW); web-page http:/ciaaw.org/.
[36] M. Schulc, M. Kostal, J. Simon, et al., Measurement of very high threshold reactions using ^{252}Cf source, Applied Radiation and Isotopes 166 (2020) 109355.
[37] M. Schulc, M. Kostal, J. Simon, et al., Constraining high energy tail of $^{235}U(n_{th},f)$ prompt fission neutron spectrum, Applied Radiation and Isotopes 166 (2020) 109313.
[38] M. Schulc, M. Petrova, T. Czakoj et al., Study of $^{239}Pu(n,f)$ prompt fission neutron spectrum, Radiation Physics and Chemistry 206 (2023) 110804.
[39] J. Adam, A.R. Balabekyan, V.S. Barashenkov et al., Spallation neutron spectrum on a massive lead/paraffin target irradiated with 1 GeV protons, Eur. Phys. J. A23 (2005) 61.
[40] J. Adam, V.S. Barashenkov, S. Ganesan et al., Measurement of the Neutron Fluence on the Spallation Source at Dubna, Kerntechnik 70 (2005) 127.
[41] A.N. Ermakov, B.S. Ishkhanov, I.M. Kapitonov, et al., Photodisintegration of heavy nuclei in the energy region above the Giant Dipole Resonance, Physics of Atomic Nuclei 73 (2010) 737.
[42] S.S. Belyshev, D.M. Filipescu, I. Gheoghe, et al., Multinucleon photonuclear reactions on ^{209}Bi: Experiment and evaluation, Eur. Phys. J. A51 (2015) 67.
[43] H. Naik, S. Singh, A. Goswami, et al., Measurement of photo-neutron cross-sections in ^{208}Pb and ^{209}Bi with 50–70 MeV bremsstrahlung, Nucl. Instr. and Meth. in Phys. Research B269 (2011) 1417.
[44] A. Wallner, M. Bichler, K. Buczak, et al., High-sensitivity isobar-free AMS measurements and reference materials for ^{55}Fe, ^{68}Ge and ^{202g}Pb, Nucl. Instr. Meth. in Phys. Res. B294 (2013) 374.
[45] M. Kostal, E. Losa, S. Simakov, et al., Impact of reactor neutron spectrum on measured spectrum averaged, Ann. of Nucl. Energy 179 (2022) 109418.
[46] M. Kostal, E. Losa, S. Simakov, et al., Measurement of spectrum averaged cross sections in LR-0 benchmark reference neutron field, Ann. of Nucl. Energy 206 (2024) 110616.

Nuclear Data Section
International Atomic Energy Agency
Vienna International Centre, P.O. Box 100
A-1400 Vienna, Austria

E-mail: nds.contact-point@iaea.org
Fax: (43-1) 26007
Telephone: (43-1) 2600 21725
Web: http://www-nds.iaea.org